Technical Report Documentation Page

1. Report No.	2. Government Accession No.	3. Recipient's Catalog No.
FHWA/TX-06/0-4863-1		

4. Title and Subtitle	5. Report Date
TRUCK INSTRUMENTATION FOR DYNAMIC LOAD MEASUREMENT	August 2006 Published: December 2007
	6. Performing Organization Code

7. Author(s)	8. Performing Organization Report No.
Emmanuel Fernando, Gerry Harrison, and Stacy Hilbrich	Report 0-4863-1

9. Performing Organization Name and Address	10. Work Unit No. (TRAIS)
Texas Transportation Institute The Texas A&M University System College Station, Texas 77843-3135	11. Contract or Grant No. Project 0-4863

12. Sponsoring Agency Name and Address	13. Type of Report and Period Covered
Texas Department of Transportation Research and Technology Implementation Office P. O. Box 5080 Austin, Texas 78763-5080	Technical Report: September 2004 – July 2006
	14. Sponsoring Agency Code

15. Supplementary Notes

Project performed in cooperation with the Texas Department of Transportation and the Federal Highway Administration.

Project Title: Characterizing the Effects of Surface Roughness on Vehicle Dynamic Loads and Pavement Life

URL: http://tti.tamu.edu/documents/0-4863-1.pdf

16. Abstract

The Texas Department of Transportation (TxDOT) is implementing a ride specification that uses profile data collected with inertial profilers for acceptance testing of the finished surface. This specification is based primarily on ride quality criteria. The objective of the present project is to establish whether gaps exist in the current specification that permit frequency components of surface profile to pass that are potentially detrimental to pavement life based on the induced dynamic loading. To carry out this objective, the work plan includes tests to measure surface profiles and vehicle dynamic loads on in-service pavement sections. This interim report documents the research efforts conducted to provide an instrumented tractor-semitrailer combination for measurement of dynamic loads and a high-speed inertial profiler for measurement of surface profiles. These test vehicles were used in this project to collect data for evaluating TxDOT's Item 585 ride specification.

17. Key Words	18. Distribution Statement
Surface Roughness, Vehicle Dynamic Loads, Truck Instrumentation, Profile Measurement, Inertial Profiler, Strain Gages	No restrictions. This document is available to the public through NTIS: National Technical Information Service Springfield, VA 22161 http://www.ntis.gov

19. Security Classif.(of this report)	20. Security Classif.(of this page)	21. No. of Pages	22. Price
Unclassified	Unclassified	80	

Form DOT F 1700.7 (8-72) Reproduction of completed page authorized

TRUCK INSTRUMENTATION FOR DYNAMIC LOAD MEASUREMENT

by

Emmanuel Fernando
Research Engineer
Texas Transportation Institute

Gerry Harrison
Research Technician
Texas Transportation Institute

and

Stacy Hilbrich
Assistant Research Engineer
Texas Transportation Institute

Report 0-4863-1
Project 0-4863
Project Title: Characterizing the Effects of Surface Roughness on Vehicle Dynamic Loads and Pavement Life

Performed in cooperation with the
Texas Department of Transportation
and the
Federal Highway Administration

August 2006
Published: December 2007

TEXAS TRANSPORTATION INSTITUTE
The Texas A&M University System
College Station, Texas 77843-3135

DISCLAIMER

The contents of this report reflect the views of the authors, who are responsible for the facts and the accuracy of the data presented. The contents do not necessarily reflect the official views or policies of the Texas Department of Transportation (TxDOT) or the Federal Highway Administration (FHWA). This report does not constitute a standard, specification, or regulation, nor is it intended for construction, bidding, or permit purposes. The United States Government and the State of Texas do not endorse products or manufacturers. Trade or manufacturers‘ names appear herein solely because they are considered essential to the object of this report. The engineer in charge of the project was Dr. Emmanuel G. Fernando, P.E. # 69614.

ACKNOWLEDGMENTS

The work reported herein was conducted as part of a research project sponsored by the Texas Department of Transportation and the Federal Highway Administration. The authors gratefully acknowledge the support and technical guidance of the project director, Mr. Brian Michalk, of the Materials and Pavements Section of TxDOT. In addition, the authors give special thanks to Dr. Roger Walker of the University of Texas at Arlington for his help in profile instrumentation. His contributions are sincerely appreciated.

TABLE OF CONTENTS

LIST OF FIGURES

Figure Page

LIST OF FIGURES (CONT.)

Figure Page

LIST OF TABLES

Table Page

CHAPTER I. INTRODUCTION

The Texas Department of Transportation (TxDOT) is implementing a new ride specification that uses profile data collected with inertial profilers for acceptance testing of the finished surface. Supplemental specification (SS) 5880 or the standard specification, Item 585, is applicable for either hot-mix asphalt or Portland cement concrete pavements. TxDOT began implementing SS 5880 in 2002. In 2003, TxDOT adopted a modified version of this smoothness specification as the standard (Item 585), and approved its publication in the 2004 standard specifications.

Both SS 5880 and Item 585 incorporate criteria on section smoothness and localized roughness to evaluate the acceptability of the finished surface. Section smoothness is evaluated at 0.1-mile intervals using the international roughness index (IRI) computed from measured profiles. In this evaluation, the average of the left and right wheel path IRIs is computed and used in the appropriate schedule to determine the pay adjustment for a given 0.1-mile section. To evaluate localized roughness, the specifications look at the differences between the average profile and its 25-ft moving average to locate bumps and dips following a modified procedure based on the methodology proposed by Fernando and Bertrand (2002).

The new standard smoothness specification (Item 585) includes pay adjustments that relate to the ride quality achieved from construction. Since the specification is based primarily on ride quality, a question to ask is, "Are there profile components not accounted for that might be detrimental to pavement life based on dynamic loading criteria?" The present research aims to answer this question by investigating the relationship between surface roughness and truck dynamic loads. The objective is to establish whether gaps exist in the current ride quality criteria implemented in Item 585 that permit frequency components of surface profile to pass that are potentially detrimental to pavement life based on the induced dynamic loading. To carry out this objective, the work plan for this project includes tests to measure surface profiles and vehicle dynamic loads on in-service pavement sections. For these tests, researchers instrumented a truck with sensors for measurement of dynamic loads and put together an inertial profiler system for measurement of surface profiles. This interim report documents the instrumentation program carried out by researchers. It is organized into the following chapters:

- Chapter I provides a brief introduction on the rationale for this project.
- Chapter II documents the truck instrumentation for measurement of dynamic loads. It presents the methodology implemented for these measurements, preliminary tests conducted to verify and develop the methodology, sensor installation, and laboratory calibrations conducted to establish calibration curves relating sensor output to measured tire loads.
- Chapter III presents the results from field tests conducted to verify the measurements from a test vehicle instrumented with an inertial profiling system at the Texas Transportation Institute (TTI). This test vehicle was used in this project to collect profile measurements for the purpose of evaluating TxDOT's current Item 585 ride specification. Prior to these measurements, researchers tested the profiler and verified that it met the certification requirements specified in TxDOT Test Method Tex-1001S.
- Chapter IV summarizes the findings from the instrumentation program.

The appendix presents the literature review conducted by researchers to gather information on the following subject areas relevant to this project:

- measurement of vehicle dynamic loads,
- truck surveys identifying truck configurations commonly used by carriers to transport goods and commodities,
- smoothness statistics for characterizing pavement smoothness based on truck damage criteria,
- vehicle transfer functions, and
- compilations of data on truck geometric, mass, and suspension properties.

CHAPTER II. DEVELOPMENT OF METHODOLOGY FOR TRUCK INSTRUMENTATION TO MEASURE DYNAMIC LOADS

The literature review conducted in this project identified strain gages as a method for instrumenting vehicles to measure dynamic loads. To use strain gages for this application, researchers:

- reviewed principles of strain gage measurement,
- conducted laboratory tests to verify their application, and
- performed small-scale experiments with an instrumented trailer to verify procedures for strain gage calibration and test a system for collecting dynamic load measurements.

This staged approach led to the instrumentation and calibration of a test vehicle that is presented in this chapter.

STRAIN GAGE PRINCIPLES

Engineering design requires information on the stresses and deformations that a structure or structural member are expected to sustain during service. For many design problems, mechanics of materials give a basis for predicting the structural response to service loads. Indeed, solutions for stresses and deformations induced under typical design loadings for simple structural members are found in the literature, and, for more complicated geometric and loading configurations, numerical techniques are available. Still, many engineering problems are encountered in practice where theoretical analysis may not be sufficient, and experimental measurements are required to verify theoretical predictions or to obtain actual measurements from laboratory or full-scale models. In most cases, force or stress cannot be measured directly, but the deformations they generate can. Thus, when an object is weighed on a scale, it is the extension of the spring that is measured, and the weight is calculated using Hooke's law with the measured spring displacement. In a similar manner, load cells have sensors that measure the deformations induced under loading that relate to the magnitude of the applied load. When the deformation is defined as the change in length per unit length of a given object, it is called strain. Of the strain-measuring systems that are available for practical applications, the most frequently used device for strain measurement is the electrical-resistance strain gage.

The term "strain gage" usually refers to a thin wire or foil, folded back and forth on itself to form a grid pattern, as illustrated in Figure 2.1. The grid pattern maximizes the amount of metallic wire or foil subject to strain in the parallel direction. The grid is bonded to a thin backing, called the carrier, which is attached directly to the test specimen. Therefore, the strain experienced by the test specimen is transferred directly to the strain gauge, which responds with a linear change in electrical resistance.

The discovery of the principle upon which the electrical-resistance strain gage is based was made in 1856 by Lord Kelvin, who observed from an experiment that the resistance of a wire increases with increasing strain according to the relationship (Dally and Riley, 1978)

$$R = \rho \frac{L}{A} \tag{2.1}$$

where R is the measured resistance in the wire of length L and cross-sectional area A having a specific resistance ρ. From this relationship, it can be shown that the strain sensitivity of any conductor derives from the change in its dimensions during loading and the change in specific resistance according to the relation

$$\frac{dR/R}{\varepsilon} = 1 + 2\nu + \frac{d\rho/\rho}{\varepsilon} \tag{2.2}$$

where ν is the Poisson's ratio of the conductor, ε is the strain and the other terms are as previously defined. In practice, the strain sensitivity is also referred to as the gage factor S_g. Thus:

$$S_g = \frac{dR/R}{\varepsilon} \approx \frac{\Delta R/R}{\varepsilon} \tag{2.3}$$

For most alloys, the gage factor varies from about 2 to 4 (Dally and Riley, 1978). Most strain gages are fabricated from a 45% nickel – 55% copper alloy known as Constantan, which has a gage factor of approximately 2. This alloy exhibits several characteristics that are useful for engineering applications. Among these are:

- The strain sensitivity is linear over a wide range of strain;
- The strain sensitivity does not change as the material goes plastic, permitting measurements of strain in both the elastic and plastic ranges of most materials;
- The alloy has a low temperature coefficient, which reduces the temperature sensitivity of the strain gage; and

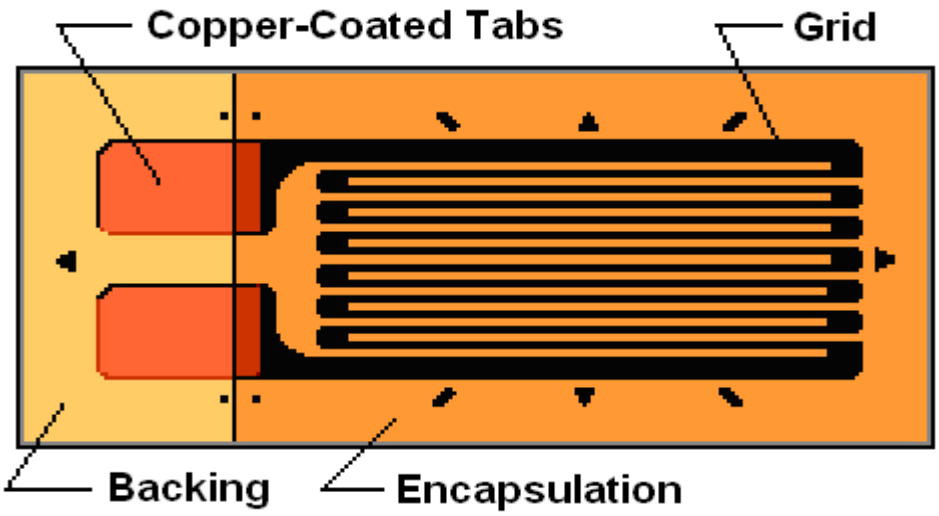

Figure 2.1. Diagram of an Electrical-Resistance Strain Gage.

- The temperature properties of selected melts of the alloy permit the production of temperature-compensated strain gages for a variety of materials on which the gages are commonly used.

In practice, the application of strain gages will require measurement of the resistance change and its conversion to strain using Eq. (2.3). This conversion is made with the gage factor that is supplied by the manufacturer of the particular sensor used in the experiment. Since the strains to be measured are typically within a few milli-strains, the resistance changes are usually too small to be measured with a simple ohmmeter. For example, at 1 percent strain, the resistance change would be only 2 percent for a sensor with a gage factor of 2. In practice, much smaller strains have to be measured. Thus, the application of strain gages will require accurate measurement of very small changes in resistance. To accomplish these measurements, a Wheatstone bridge is typically used. This method permits both static and dynamic strain gage measurements. It is interesting to note that this is the same method Lord Kelvin used to measure resistance changes in the classic experiment he conducted in the mid-19th century.

Figure 2.2 illustrates the Wheatstone bridge circuit. Up to four strain gages may be connected to the four arms of the bridge. When the gage resistance is changed by strain, the bridge becomes unbalanced, resulting in a voltage change that is easily measured. For a Wheatstone bridge with a constant voltage excitation V and resistances R_1, R_2, R_3, and R_4, the

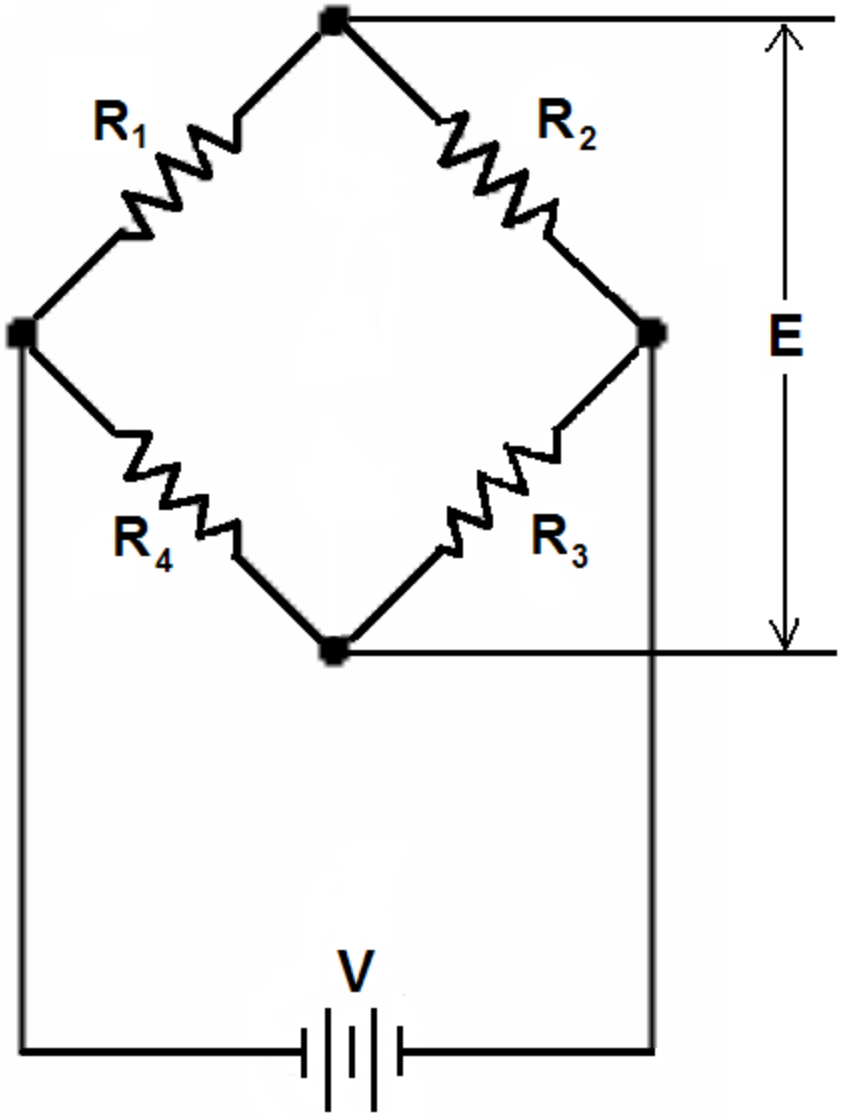

Figure 2.2. Wheatstone Bridge Circuit with Constant Voltage Excitation.

voltage change ΔE is related to the change in resistance ΔR_i in each bridge arm i by the relation (Dally and Riley, 1978):

$$\Delta E = V \frac{R_1 R_2}{(R_1 + R_2)^2} \left(\frac{\Delta R_1}{R_1} - \frac{\Delta R_2}{R_2} + \frac{\Delta R_3}{R_3} - \frac{\Delta R_4}{R_4} \right) \tag{2.4}$$

For a multiple gage circuit with n gages (n = 1, 2, 3, or 4) whose outputs sum when placed in the bridge circuit, Eq. (2.4) can be rewritten as

$$\Delta E = V \frac{R_1 R_2}{(R_1 + R_2)^2} n \frac{\Delta R}{R} \tag{2.5}$$

where ΔR is the change in the bridge resistance and R is the nominal resistance of the bridge elements. The bridge circuit sensitivity S_c is defined as the change in voltage per unit strain. Setting $r = R_1/R_2$, this parameter is determined from Eqs. (2.3) and (2.5) as follows:

$$S_c = \frac{\Delta E}{\varepsilon} = V \frac{r}{(1+r)^2} n S_g \qquad (2.6)$$

It can be shown that the maximum circuit sensitivity is achieved when $r = 1$. With one strain gage connected to the Wheatstone bridge, Eq. (2.6) gives the sensitivity of this configuration as $S_g V/4$, compared to a sensitivity of $S_g V$ for a four-arm active configuration. The four-arm active bridge is of particular interest as it was the bridge configuration used for dynamic load measurements with the instrumented tractor-semitrailer in this project. In addition to providing the highest sensitivity, this bridge arrangement is also temperature-compensated and rejects both axial and bending strains for applications involving shear strain measurement. For this bridge configuration, the strain corresponding to the measured voltage change in the Wheatstone bridge is determined from the formula:

$$\varepsilon = \frac{\Delta E}{S_g V} \qquad (2.7)$$

Prior to instrumenting a tractor-semitrailer with strain gages for dynamic load measurements, researchers conducted laboratory and field tests to verify the application of the strain gage principles presented in this section. Specifically, the researchers verified the principles presented in the laboratory through an experiment that they conducted with a simple shear beam load cell. Following up on this experiment, researchers instrumented and conducted laboratory and field tests on a small trailer to verify the intended method of measuring dynamic loads using shear strain gages. The tests performed are presented in the subsequent sections.

SHEAR BEAM LOAD CELL EXPERIMENT

For a prismatic cantilevered beam of solid rectangular cross-section with a load W at its free end, the shear stress τ at any given cross-section along its length is given by the formula

$$\tau = \frac{W Q}{I b} \qquad (2.8)$$

where

Q = area moment about the neutral axis,

I = moment of inertia about the neutral axis, and

b = width of the beam.

For a solid rectangular cross-section of width b and height h, Q and I are given by the following equations:

$$Q = \frac{bh^2}{8} \tag{2.9}$$

$$I = \frac{bh^3}{12} \tag{2.10}$$

Substituting Eqs. (2.9) and (2.10) in Eq. (2.8) and considering that the shear stress τ equals the shear modulus G multiplied by the shear strain γ, the following equation for computing the load W is obtained:

$$W = \frac{2bhG\gamma}{3} \tag{2.11}$$

To verify the application of shear strain gages for load measurement, researchers instrumented a steel bar of rectangular cross-section with a pair of two-element 90° strain rosettes. Figure 2.3 illustrates the strain rosette used for this laboratory experiment. Two such gages were mounted on opposite faces of the rectangular steel bar in a four-arm active or full bridge configuration. The steel bar was then clamped to a work bench as shown in Figure 2.4 and used to measure a known set of weights suspended at the free end of the bar. Researchers note that the bridge was zeroed prior to placing the circular disks of known weights at the free end of the bar (see Figure 2.4). This action removes the initial strain due to the weight of the bar and the weight of the disk holder.

The test setup included a signal conditioner, data acquisition module, and a notebook computer. The strain rosettes were wired to the signal conditioner, which provided the excitation voltage for the test, amplified the signal from the strain gages, and measured the voltage change as the bar was loaded. Data from the signal conditioner were fed to the data acquisition module, which in turn was connected to the notebook computer via a universal serial bus (USB) cable. A data acquisition program running on the notebook computer collected and recorded voltage readings during the test. From these measurements, researchers computed a shear strain of about 8 με.

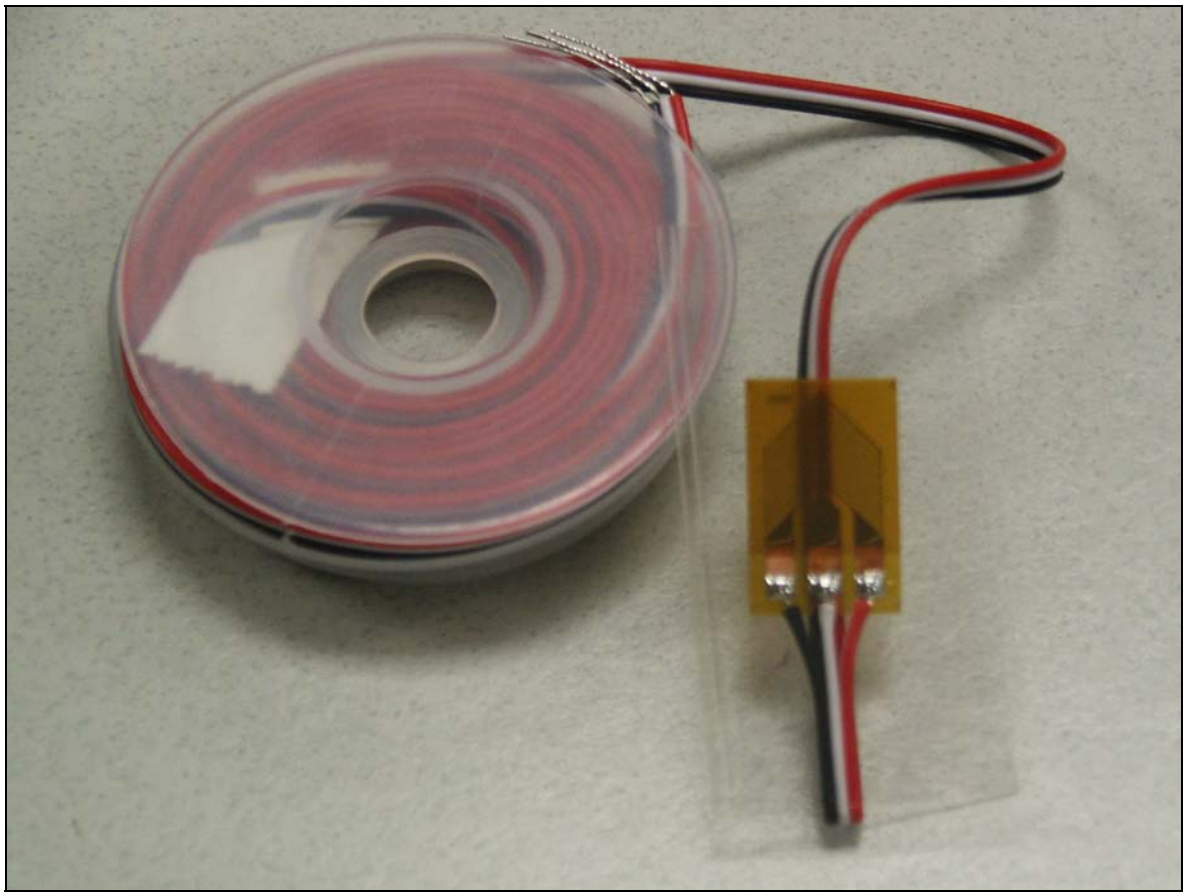

Figure 2.3. Shear Strain Gage Used for Tests.

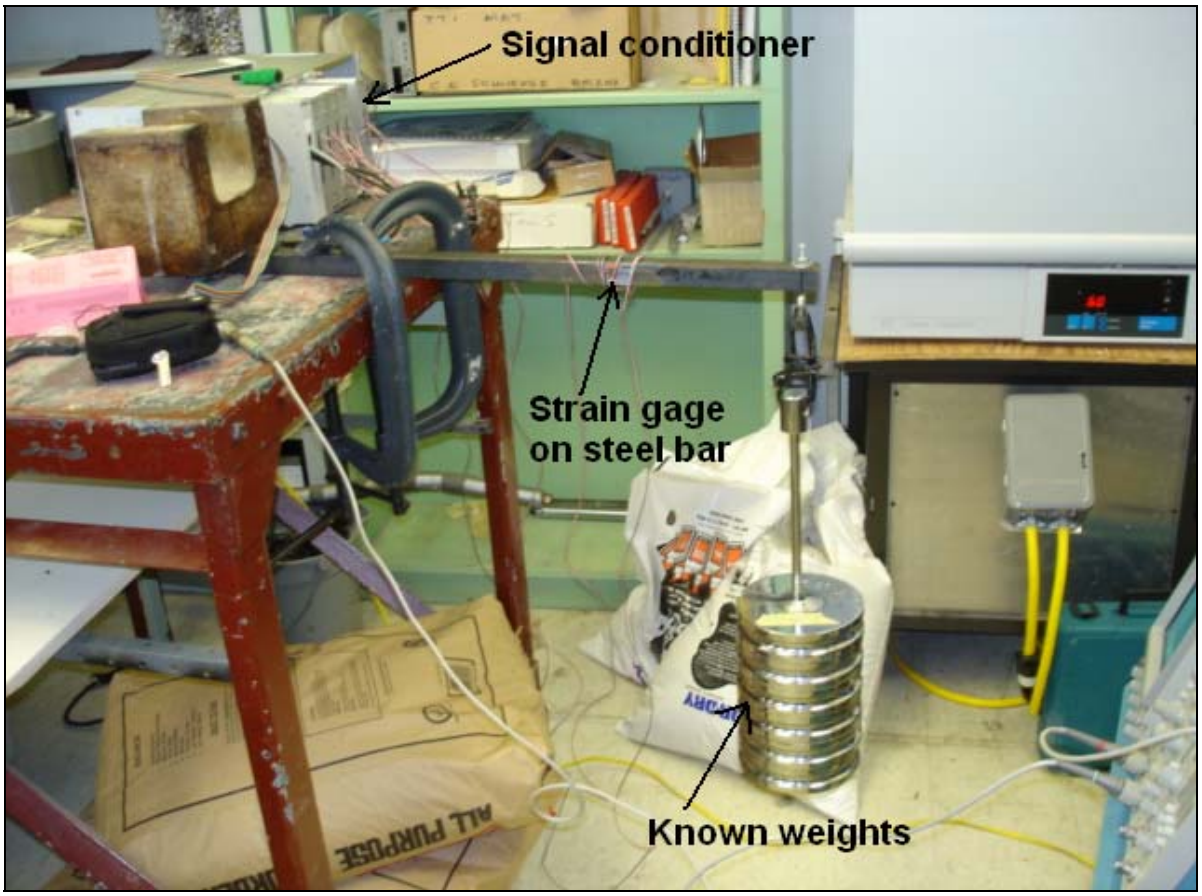

Figure 2.4. Shear Beam Load Cell Experimental Setup.

Given the Young's modulus E_{mod} for the bar of 29,000 ksi, researchers computed the corresponding shear modulus from the equation:

$$G = \frac{E_{mod}}{2(1+\nu)} \qquad (2.12)$$

This calculation gave a shear modulus of 11,284 ksi for a Poisson's ratio ν of 0.285 for the steel bar. Since the cross-sectional area ($b \times h$) of the bar is 1 inch^2, the total weight of the circular disks at the free end was computed to be 60.2 lb from Eq. (2.11). This value compares very closely with the reference weight of 60 lb placed on the bar. The close agreement verifies the correct application of the strain gage principles in this laboratory experiment.

SMALL-SCALE TESTING WITH AN INSTRUMENTED TRAILER

Following up on the laboratory test with the shear beam load cell, researchers instrumented a small trailer with shear strain gages to verify the intended method of

measuring dynamic loads. Considering the high cost of renting, instrumenting, and calibrating an 18-wheeler for the tests planned in this project, researchers believed that a small-scale experiment to verify the intended method of dynamic load measurement was a prudent step to take. For this experiment, researchers instrumented the single-axle trailer shown in Figure 2.5. For this instrumentation, researchers instrumented the left side of the trailer axle with a pair of two-element 90° strain rosettes (Figure 2.3) of the same make and model used in the shear beam load cell experiment. This gage is made of Constantan alloy that is self-temperature compensated for tests on cast iron and steel materials. As shown in Figure 2.3, the sensor has two grids arranged in a chevron pattern that sense normal strains in perpendicular directions. The grids have a common connection for use in half-bridge circuits, which yield the shear strain directly. Two such gages were mounted on the left side of the trailer axle on opposite faces and were connected to a signal conditioner in a full bridge configuration. The gages were mounted between the leaf-spring suspension and the inside of the left tire as shown in Figure 2.6. The installation procedure included the following steps:

Figure 2.5. Small-Scale Trailer Used to Verify Strain Measurement Methodology.

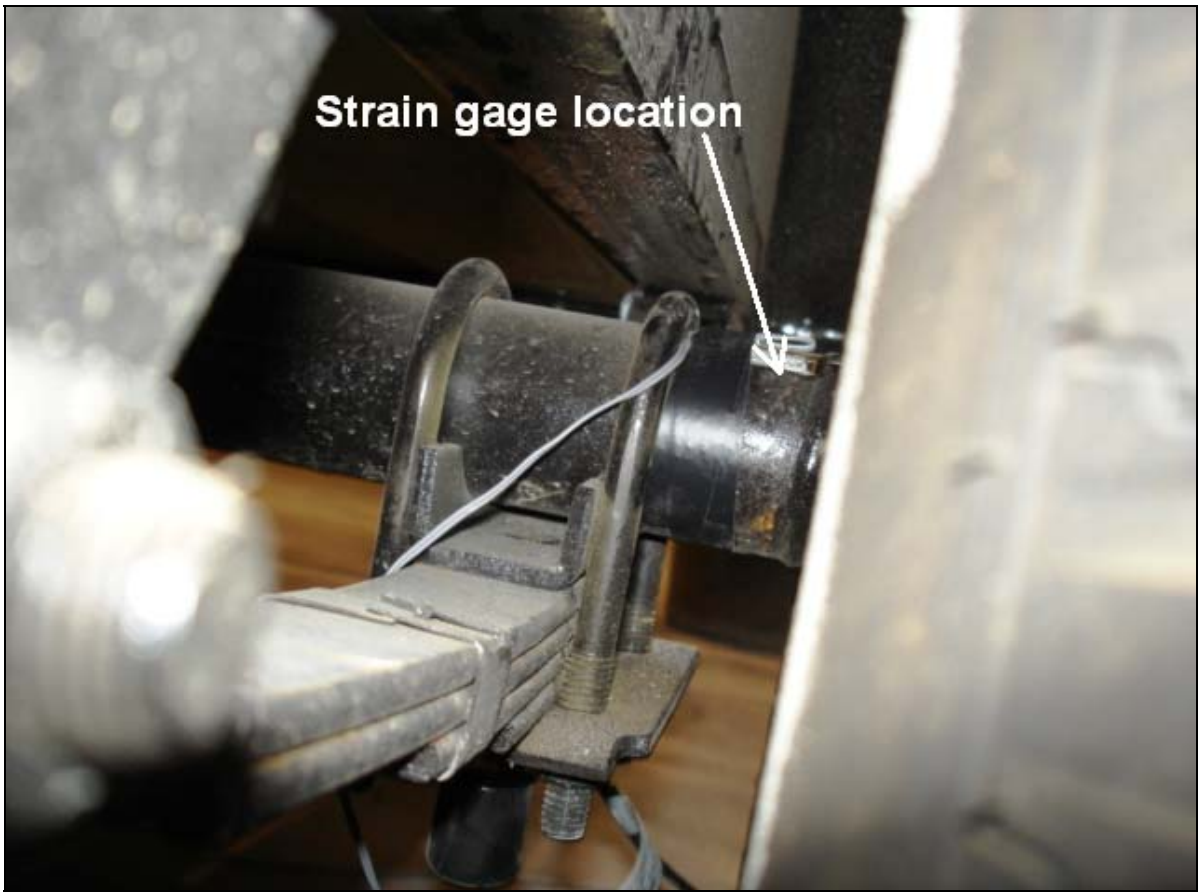

Figure 2.6. Strain Gages Positioned between Suspension and Tire of Small Trailer.

- Removed paint from the axle by sanding down to the metal;
- Cleaned sanded area with a light acid solution to remove oil and contamination. Rinsed with an acid neutralizer solution;
- Positioned the gages on the axle where measurements were to be made and held temporarily in place with Mylar tape;
- Pulled back the Mylar tape and applied a small amount of AE-10 glue on the axle. Slowly replaced Mylar tape with the gages onto the axle, carefully squeezing out the glue so as to get a thin film of the adhesive between the gages and the axle surface;
- Placed the release film, pressure pad, and clamping plate on top of the gages. Held these items firmly in place with a cable tie long enough to go around the axle. Let the glue cure for at least 24 hours; and
- Upon curing, removed the clamping plate, pressure pad, release film, and Mylar tape. Protected the strain gages from road debris during testing by applying a small amount of silicone sealant on top of the gages.

In addition to the strain gages, researchers included two other sensors in the data acquisition system for field testing. One was a distance encoder that researchers attached to the left wheel hub of the towing vehicle to tie the strain measurements to ground distance. The other was a start sensor to locate the start of the section to be tested with the instrumented trailer.

Researchers determined the load calibration curve for the strain gages mounted to the trailer using an MTS loading system. For this laboratory calibration, the loading ram of the MTS was used to apply load at the middle of the axle, as illustrated in Figure 2.5. As loads were applied, corresponding strains were determined from the voltage readings measured with the signal conditioner and recorded with the data acquisition software. These voltage readings were converted to strains using Eq. (2.7) with S_g = 2.065 and V = 10 volts. In addition, the force underneath each tire was determined with a load cell positioned under the tire, as illustrated in Figure 2.7. From these load and strain measurements, researchers determined the load calibration curve given in Figure 2.8. As observed, the load-strain relationship is linear over the range of loads at which the trailer was tested, and the regression line fits the data points quite well. This linear relationship is given by the equation:

$$\text{Left tire load (lb)} = -18.9 - 15.1 \times \text{shear strain } (\mu\varepsilon) \qquad (2.13)$$

The above equation has a coefficient of determination (R^2) of 99.5 percent and a standard error of the estimate (SEE) of 22.7 lb.

After the laboratory calibration, researchers collected data with the trailer on a weigh-in-motion (WIM) site located along SH6 close to the intersection with FM60 in College Station. Figures 2.9 to 2.13 plot the dynamic tire loads determined from the left strain gage readings collected from five runs made with the instrumented trailer. Also shown is the WIM measurement for each run. Researchers note the following observations from these charts:

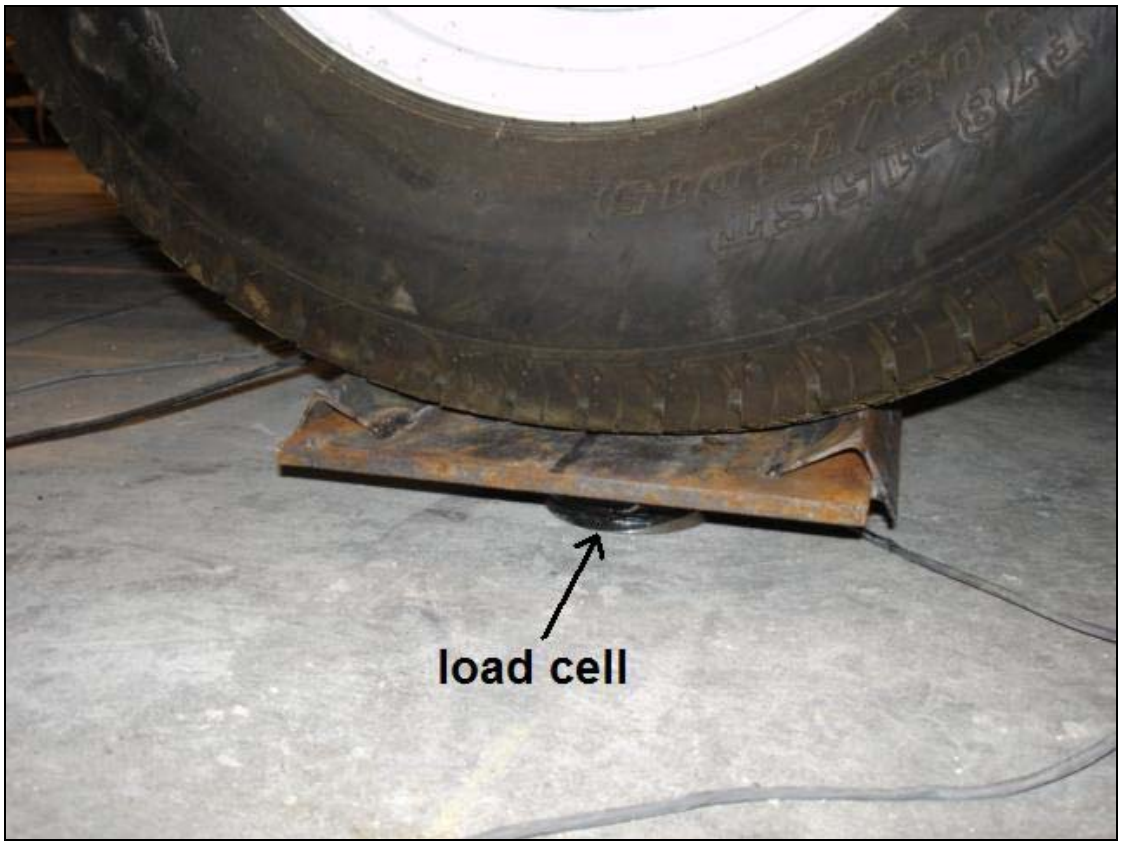

Figure 2.7. Load Cell Placed under Tire during Calibration of Small Trailer.

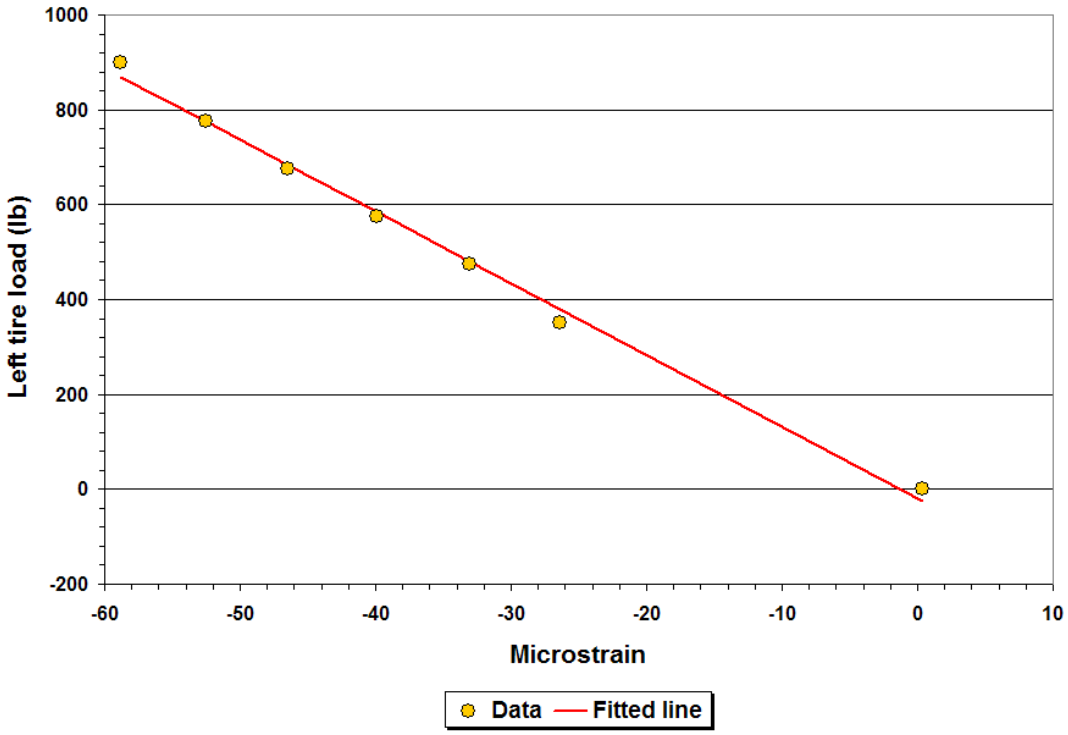

Figure 2.8. Data from Laboratory Calibration of Small Trailer.

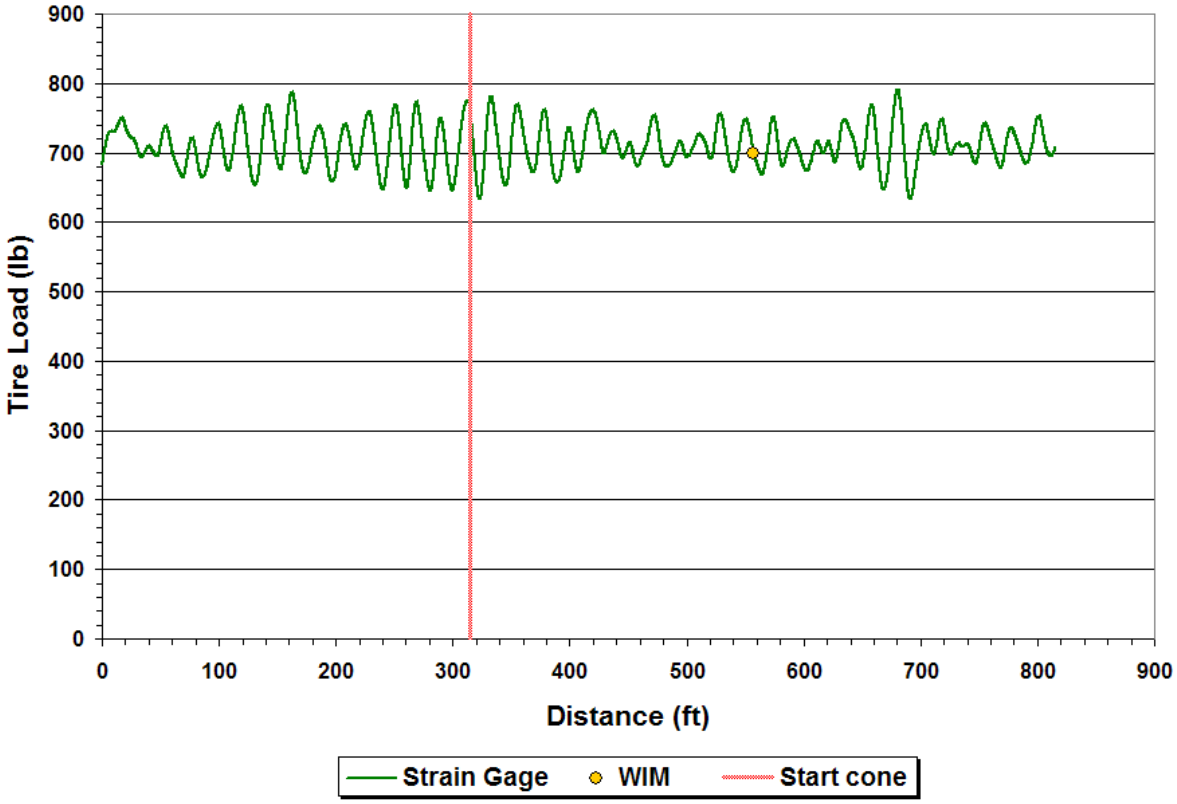

Figure 2.9. Dynamic Loads on Left Tire from Run 1 of Small Trailer on SH6 WIM Site.

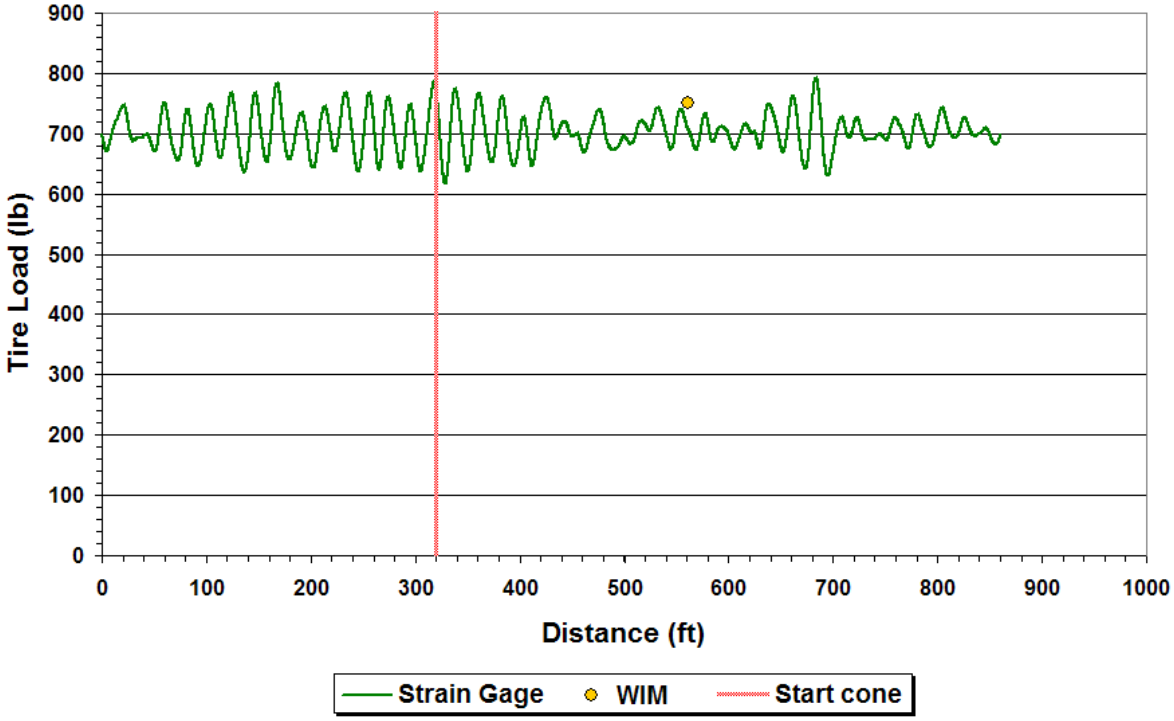

Figure 2.10. Dynamic Loads on Left Tire from Run 2 of Small Trailer on SH6 WIM Site.

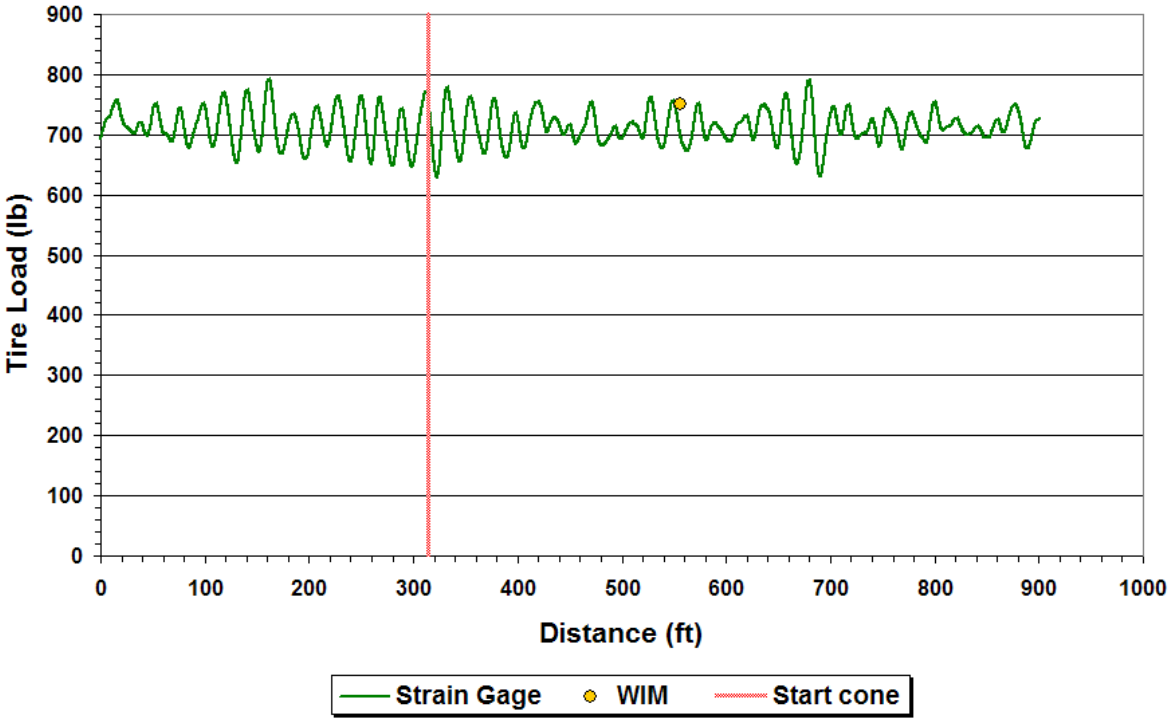

Figure 2.11. Dynamic Loads on Left Tire from Run 3 of Small Trailer on SH6 WIM Site.

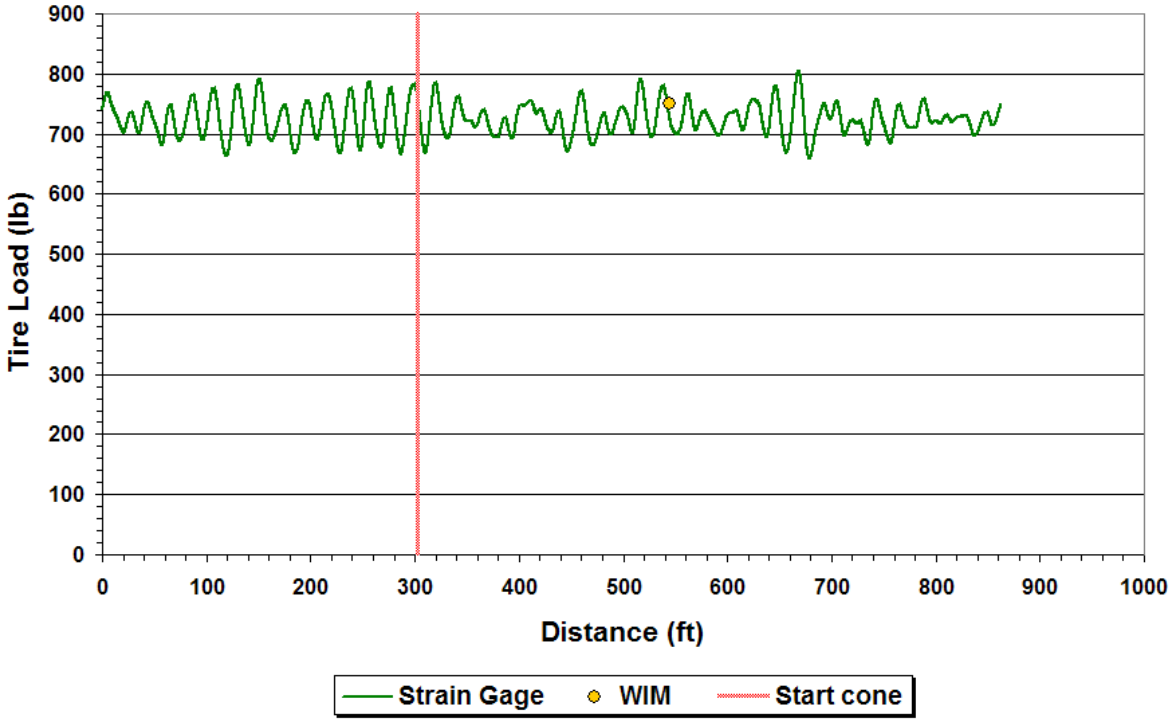

Figure 2.12. Dynamic Loads on Left Tire from Run 4 of Small Trailer on SH6 WIM Site.

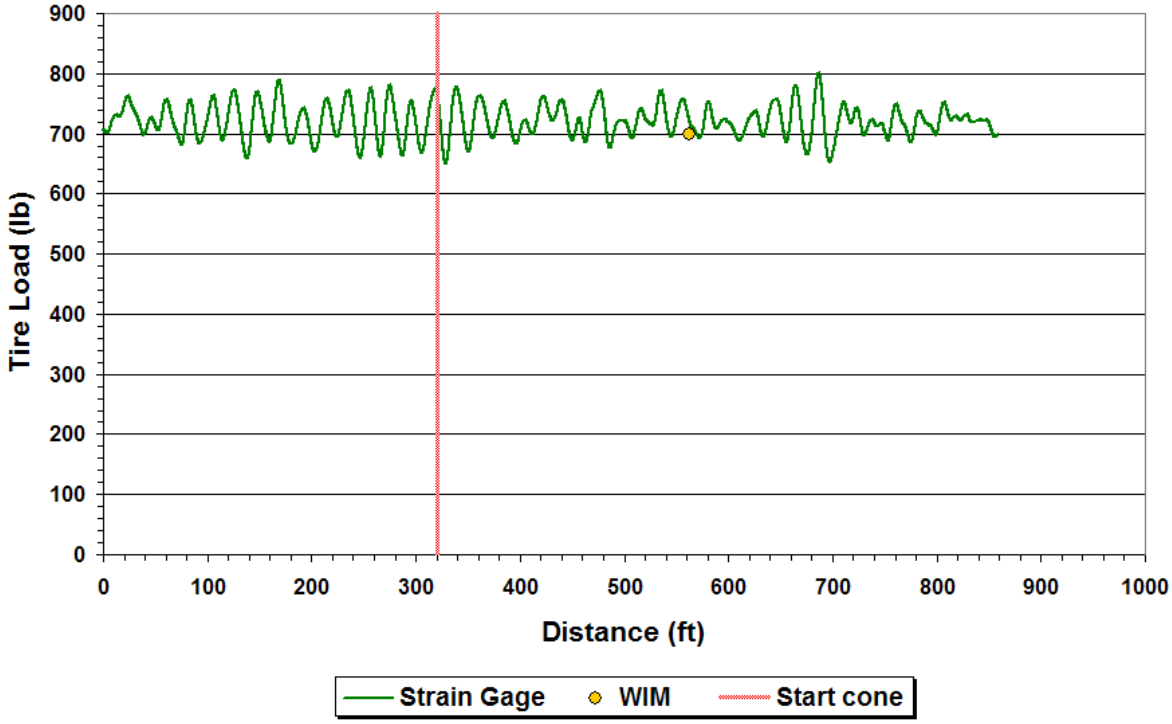

Figure 2.13. Dynamic Loads on Left Tire from Run 5 of Small Trailer on SH6 WIM Site.

- The dynamic tire loads vary closely about the static tire load of 700 lb,
- The dynamic tire loads determined around the vicinity of the WIM sensor are in reasonable agreement with the corresponding WIM measurement on each of the five runs, and
- The load measurements show similar patterns between repeat runs.

Table 2.1 compares the WIM readings with the corresponding dynamic tire loads determined from the strain gages. A statistical test of the difference between the means indicated no significant difference (at the 5 percent level) between the averages of the WIM readings and the dynamic loads determined from the strain gages. With respect to the static tire load of 700 lb, the WIM sensor readings varied from zero to about 7 percent of the static load on the runs made. For the instrumented trailer, the percent difference ranged from about zero to 3 percent. Researchers note that the American Society for Testing and Materials (ASTM) stipulates a requirement of ±20 percent on wheel load measurements for Type III WIM systems in its ASTM E-1318 specification. The results presented should not be interpreted to mean that the WIM system classifies as a Type III. Rather, the specification is simply given to provide a reference with which to judge the level of agreement between the static and

Table 2.1. Comparison of Vertical Dynamic Tire Loads.

Run	Vertical Dynamic Tire Load (lb)	
	WIM Sensor	Instrumented Trailer
1	700	703
2	750	706
3	750	699
4	750	724
5	700	718

dynamic tire loads from the field test conducted. Based on the specified tolerance of ±20 percent and the results obtained, the agreement is good in the opinion of the researchers. This good agreement is consistent with the relatively small variability observed in the dynamic tire loads, as reflected in coefficients of variation ranging from 2.7 to 3.4 percent over an interval that spans ±60-ft of the WIM sensor. This interval covers a little more than twice the total wheel base (27 ft) of the test vehicle on each side of the WIM sensor. Examination of inertial profile data collected at the WIM site also revealed no defects over this interval that would have excited the vehicle dynamics and affected the load measurements at the vicinity of the WIM sensor.

Considering the good agreement between the WIM readings and the dynamic load measurements from the test vehicle, researchers were satisfied that the field test verified the methodology for using strain gages to measure dynamic tire loads. While the results are based on data taken from a relatively smooth pavement, tests to evaluate TxDOT's existing ride specification will cover pavements with surface smoothness considered representative of new construction or resurfacing projects. Consequently, researchers proceeded with instrumenting and calibrating a tractor-semitrailer following the same approach used with the small-scale trailer testing presented in this section.

INSTRUMENTATION AND CALIBRATION OF TRACTOR-SEMITRAILER COMBINATION

Figure 2.14 shows a picture of the tractor-semitrailer combination that researchers tested in this project. The selection of a vehicle combination for instrumentation and testing considered the findings of a truck survey conducted by Wang et al. (2000) in an earlier TxDOT project. In that survey, researchers identified the tractor-semitrailer as the most common truck configuration used by truck carriers in Texas. The survey also identified radial tires as the most common truck tire used by truckers, and leaf and air springs as the

Figure 2.14. Instrumentation and Calibration of Test Vehicle in the Laboratory.

most popular suspensions. These suspensions were never observed to be on the same axle for the trucks that were sampled, with air spring suspensions commonly found on the drive axles, and semi-elliptic leaf springs on the trailer axles. In view of these findings, researchers selected an 18-wheeler with air bag suspensions on the drive axles and leaf springs on the trailer axles for instrumentation and testing in this project. In terms of truck tire use, Wang et al. found that the 11R24.5 tire was most frequently used on steering axles, while the 295/75R22.5 radial tire was most often seen on non-steering axles. These same tires were specified on the vehicle instrumented by researchers on this project.

As shown in Figure 2.14, the 18-wheeler was driven into the high-bay structural and materials testing laboratory of the civil engineering department at Texas A&M University. This facility provided ample space and test equipment for instrumenting and calibrating the tractor-semitrailer in an air-conditioned environment. The instrumentation work covered the installation of the same types of sensors (shear strain gages, distance encoder, and start sensor) used for the small-scale trailer testing, except that more strain gages were used to

permit measurement of tire loads for all five axles of the tractor-semitrailer. Additionally, researchers added thermocouple sensors to monitor temperatures at the steering, drive, and trailer axle assemblies during testing. Researchers note that temperature sensitivity of the strain measurements is not considered to be an issue in view of the temperature-compensated strain gages and the full bridge configuration used in the truck instrumentation. Nevertheless, researchers decided to add thermocouples for monitoring test temperatures, which might later prove useful for data analysis and interpretation.

Figure 2.15 shows the layout of the sensors, signal conditioning, and data acquisition devices on the test vehicle. All strain gages were wired to the same signal conditioner used in the small-scale trailer testing. This conditioner amplified the gage readings and measured the voltage changes in all strain gage channels during testing. Data from all channels (including the distance encoder, start sensor, and thermocouples) fed into a 16-bit Model 9834 Data Translation module with a 500 KHz maximum sampling rate. This module was connected to a notebook computer for data collection via a USB cable. A general purpose data acquisition program was used to read and record data from all channels during testing. Researchers specified a sampling rate of 4 KHz for each channel on test runs made to collect dynamic load measurements on in-service pavement sections.

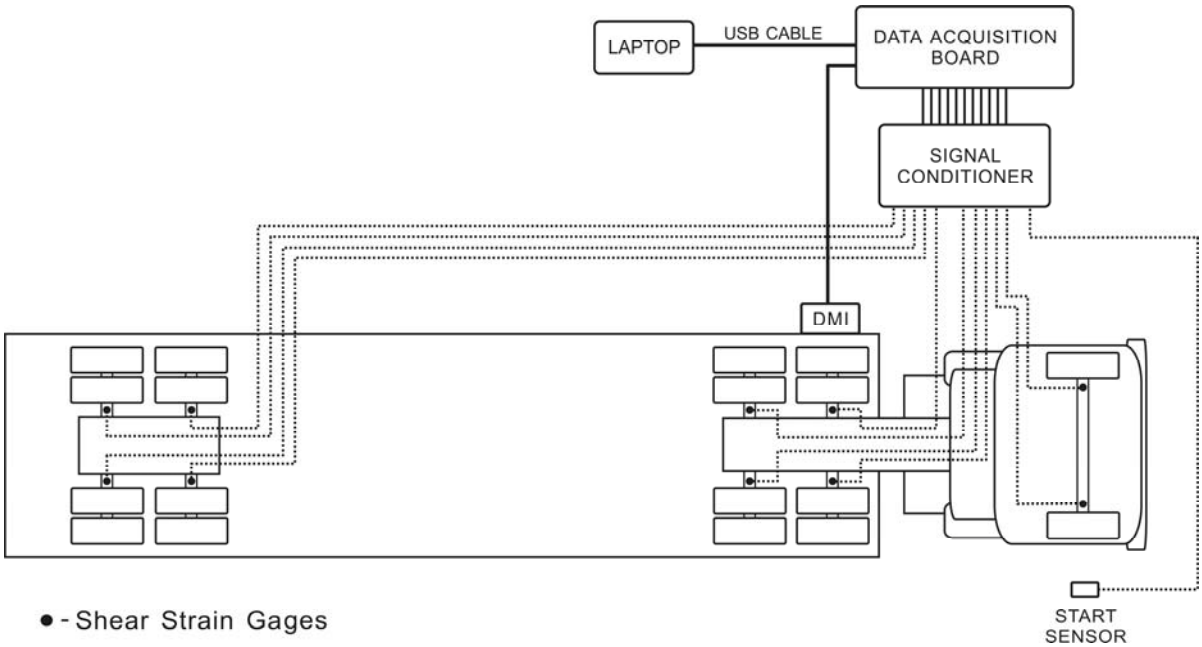

Figure 2.15. Layout of Sensors, Signal Conditioning, and Data Acquisition Devices on Instrumented Truck.

Similar to the installation of strain gages for the small-scale trailer testing, the gages were mounted on the 18-wheeler between the suspension and inside tire of each axle as illustrated in Figures 2.16 and 2.17. Two shear strain gages were mounted on each side of the axle on opposite faces, one toward the front and the other toward the rear of the test vehicle. Each strain gage pair was wired in a full bridge configuration for dynamic load measurement on that side of the given axle.

After installation of the gages and set up of the data acquisition system, researchers conducted calibrations to determine the load-strain relationships for the different gages. This calibration was conducted in a similar manner as the small trailer calibration except that more axles were tested, beginning with the trailer tandem axle, then the drive, and finally the steering axle. For calibrating each axle group, researchers positioned a loading plate (Figure 2.18) on the trailer flatbed at the geometric center of the tandem axle assembly where gages were to be calibrated. In this way, the applied vertical loads to the loading plate were distributed primarily to the axle group that was being calibrated. To measure the vertical tire loads during calibration, technicians used the loading crane of the high-bay laboratory to lift the axle assembly and position load cells underneath each dual tire (Figure 2.19). Researchers then recorded the readings from the strain gages on the axle group along with the corresponding vertical tire loads from the load cells during calibration.

Prior to calibrating the strain gages, researchers calibrated the load cells by determining the relationship between the readings from each load cell and the corresponding loads measured with the reference load cell maintained by the high-bay structural and materials testing laboratory. The authors note that the calibration of the reference load cell is National Institute of Standards and Technology (NIST) traceable. During calibration, the voltage readings from the test load cells were recorded along with the corresponding load magnitudes measured with the reference load cell. Figures 2.20 to 2.23 show the calibration equations determined from these tests. The relationships show a high degree of linearity over the range of loads at which the calibrations were conducted. In addition, the regression line fits the test data for each load cell very well. Thus, researchers used the relationships shown to calibrate the strain gages mounted on the tractor-semitrailer for measurement of dynamic tire loads.

During calibration, researchers used a 100-kip MTS system to apply loads to the axle assembly through the loading plate positioned at the geometric center of the axle assembly

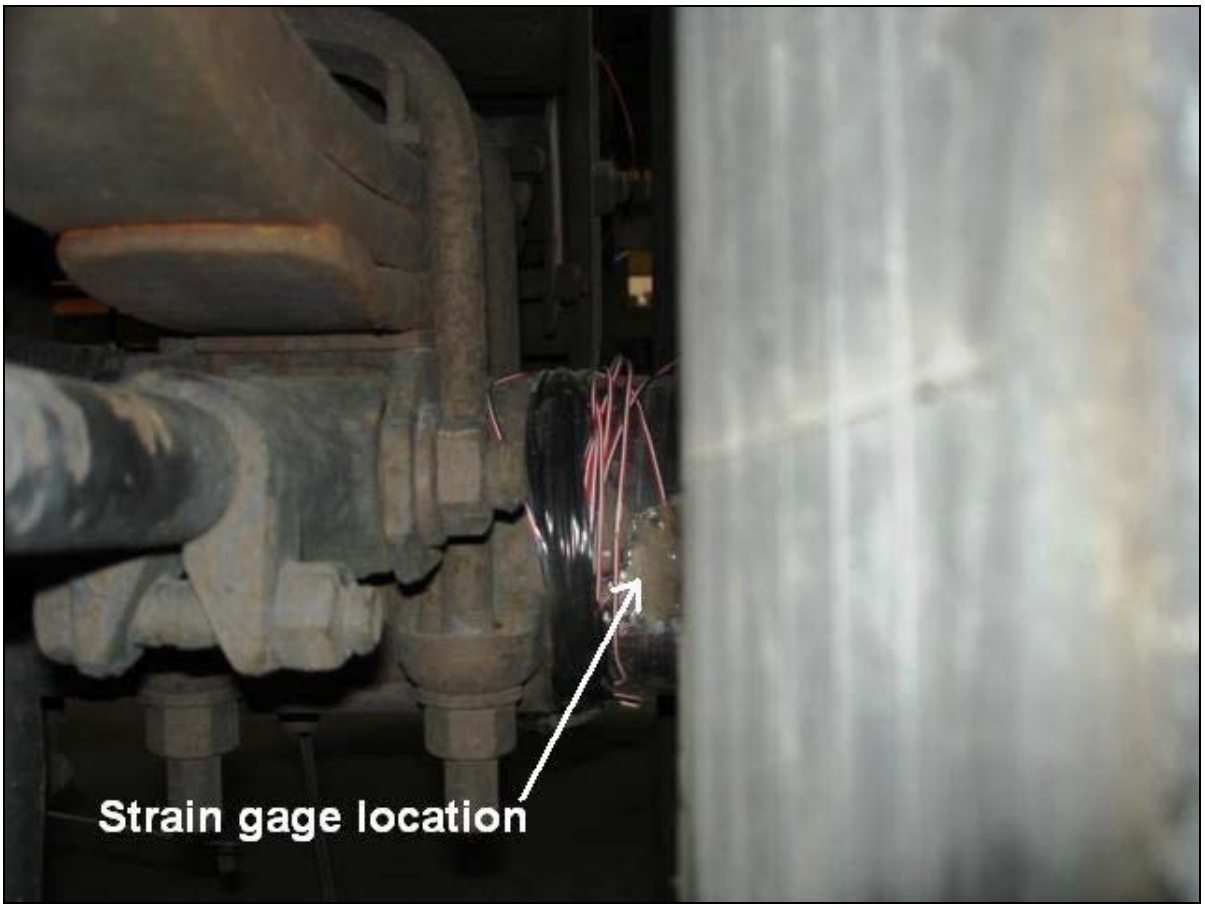

Figure 2.16. Strain Gage Mounted on Trailer Axle.

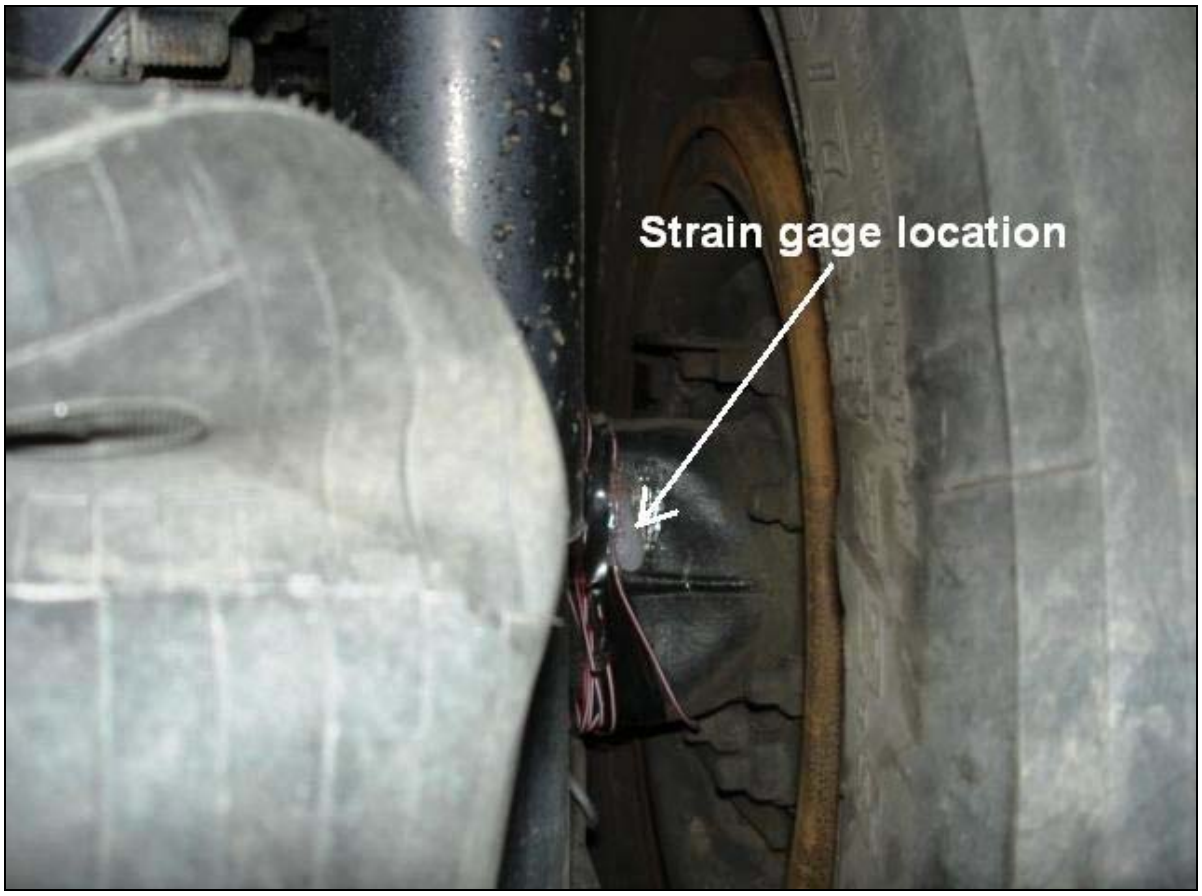

Figure 2.17. Strain Gage Mounted on Drive Axle.

Figure 2.18. Application of Load to Axle Assembly through Loading Plate. (axle assembly underneath the loading plate and load ram)

Figure 2.19. Load Cells Positioned under Dual Tires of Trailer Axle Assembly.

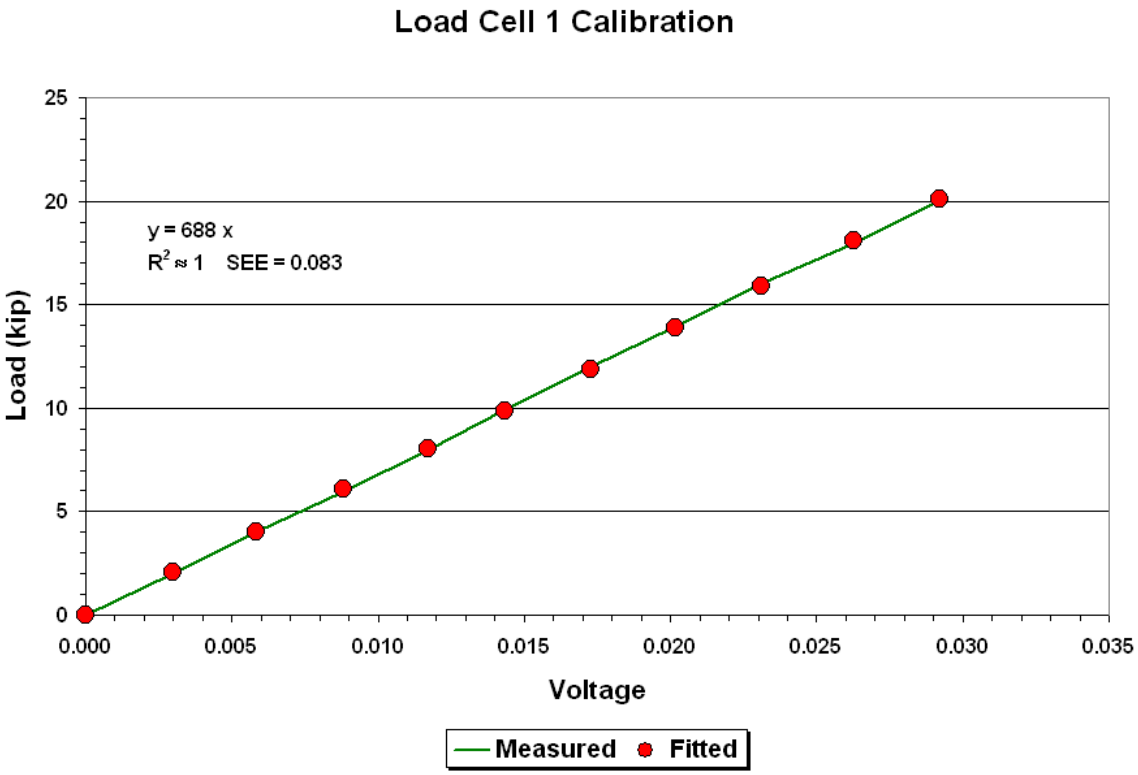

Figure 2.20. Calibration Results for Load Cell #1.

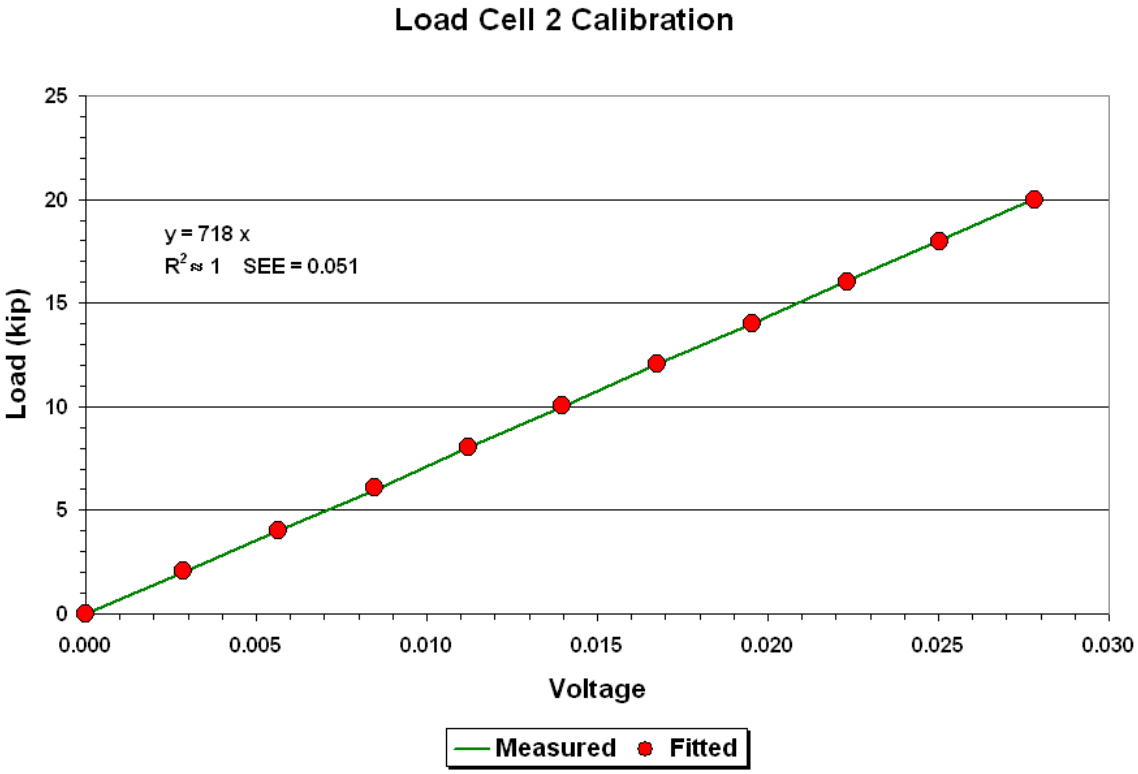

Figure 2.21. Calibration Results for Load Cell #2.

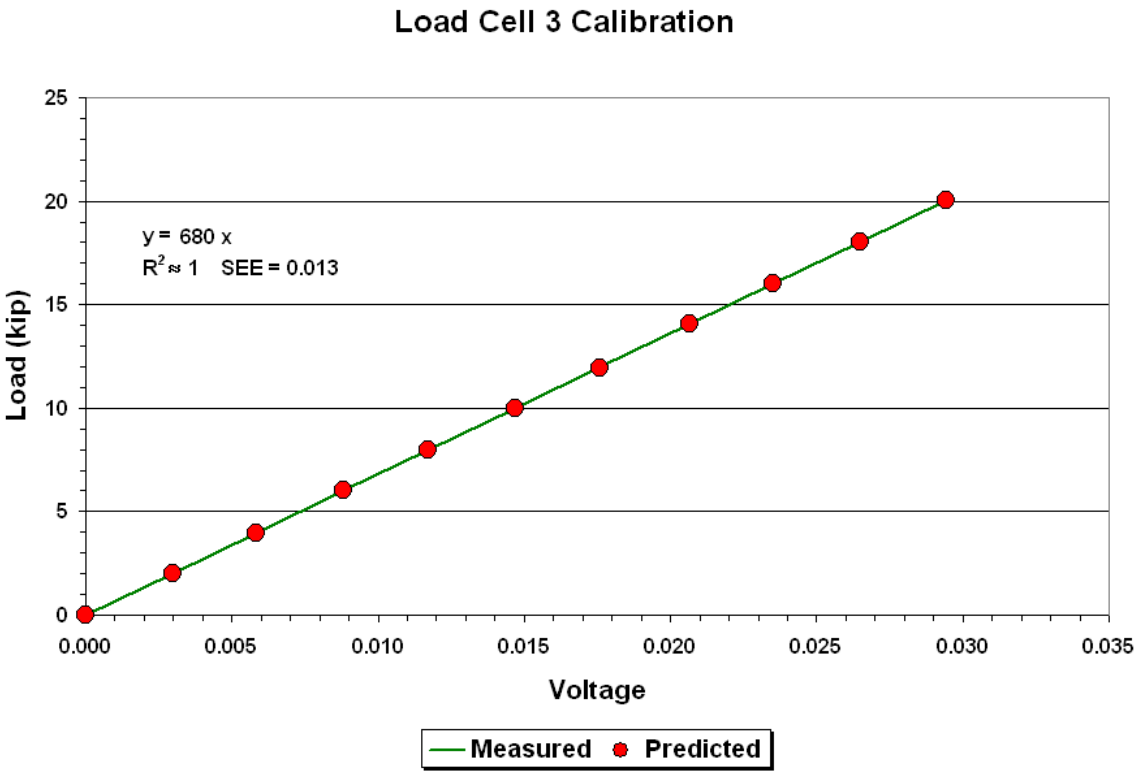

Figure 2.22. Calibration Results for Load Cell #3.

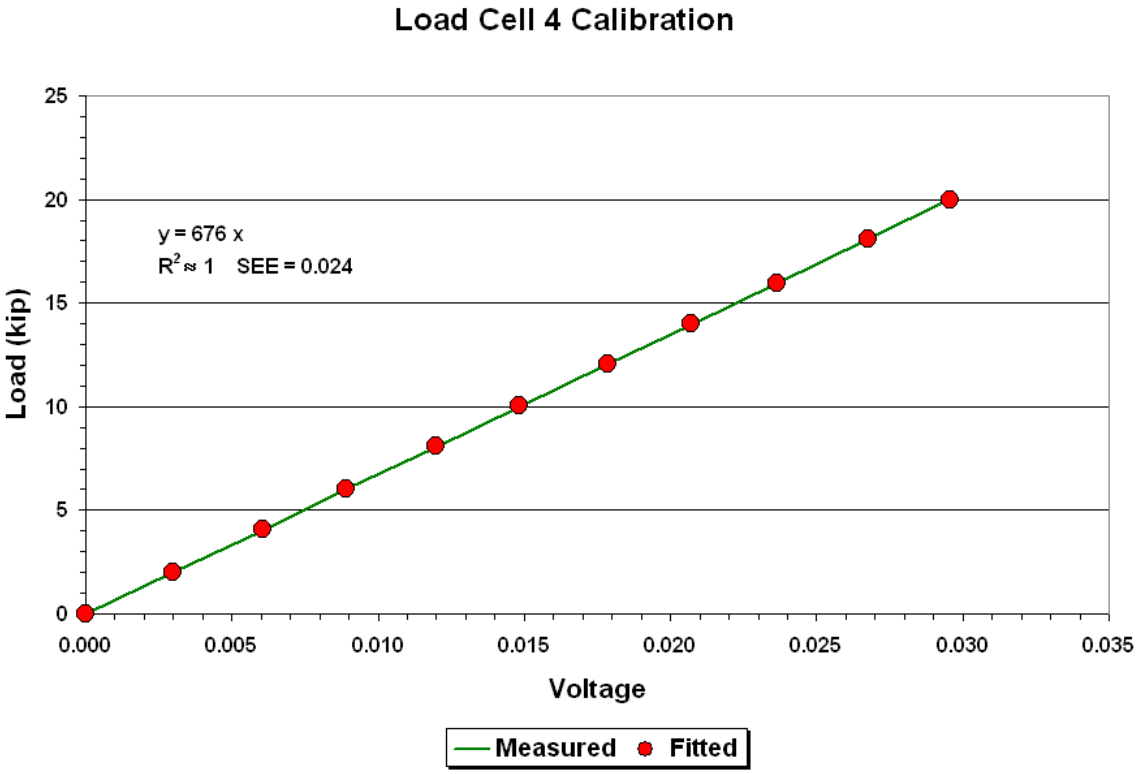

Figure 2.23. Calibration Results for Load Cell #4.

where gages were to be calibrated. The first step in the calibration was to zero the strain gages and load cells. This step was accomplished with the axle assembly raised above ground using the loading crane. After zeroing the strain gages and load cells, technicians carefully lowered the axle assembly back onto the load cells. The initial strain and load cell readings were then recorded with no other loads applied to the trailer. Subsequently, researchers applied a series of loads to the axle group using the 100-kip MTS system. At each load level, strain gage and load cell readings were recorded to collect data for determining the calibration curves of the different gages mounted on the axle assembly tested. This loading sequence was followed by an unloading sequence during which readings were taken as the loads were reduced.

Figures 2.24 to 2.27 illustrate the load-strain relationships determined from calibration of the strain gages mounted on the trailer axles. It is observed that the data exhibit a strong linear relationship between the strain gage readings and the tire load measurements for the range of loads applied. Note also the difference in signs of the shear strains between the left and right sides of each axle. This difference is expected based on mechanics principles.

Researchers used the same procedure for calibrating the trailer gages to calibrate the gages on the drive axles. Figures 2.28 to 2.31 show the calibration relationships determined for drive axle strain gages. Again, the test data exhibit a strong linear relationship between the strain gage readings and the measured tire loads. The regression line also fits the test data for each drive axle strain gage quite well, in the authors' opinion.

For the steering, there was no way of applying the load directly on top of the axle, either from the front of the tractor or from inside the engine compartment. Since the vehicle was rented, modifications were not possible. Consequently, the calibration data for the steering axle were collected with the loads applied through the drive axles. During this process, the loads transmitted to the steering axle were measured with load cells placed underneath its left and right tires. To keep the tractor level, researchers placed spacers underneath the drive axles. While it was not possible to load the steering axle directly, researchers are of the opinion that the method used to calibrate the gages on the steering axle simulated more closely the way loads are transmitted or distributed to this axle in practice.

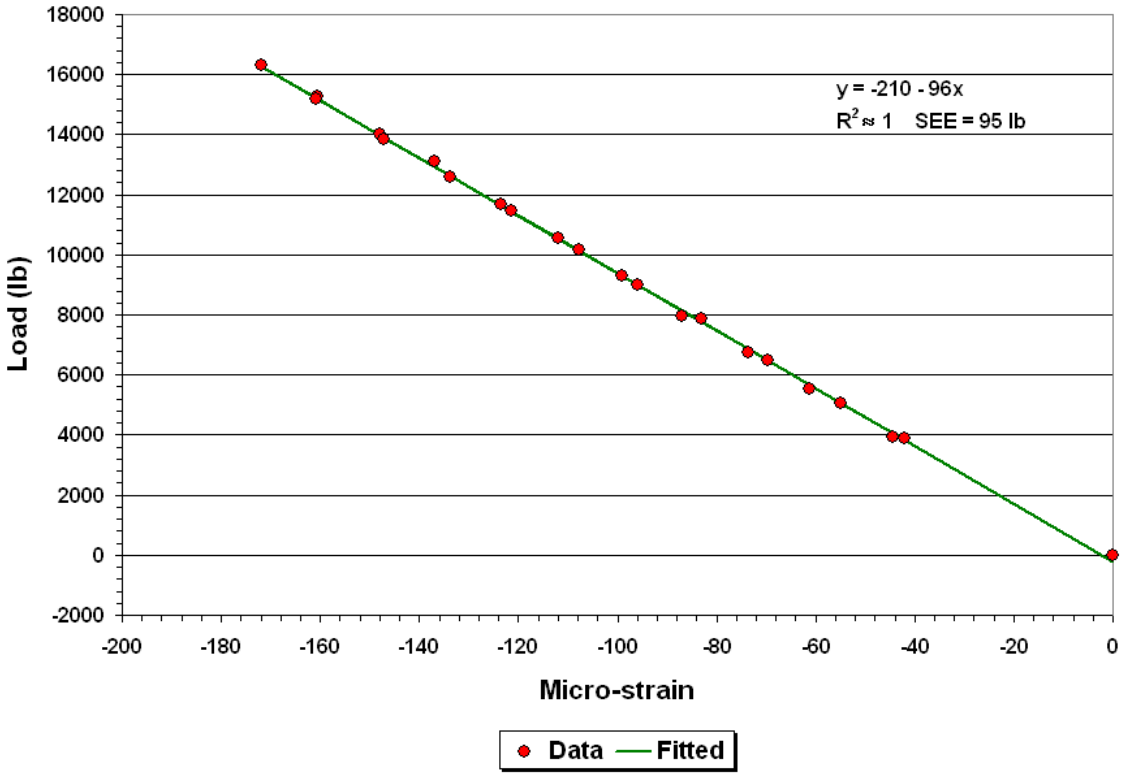

Figure 2.24. Strain Gage Calibration Curve for Left Side of Trailer Lead Axle.

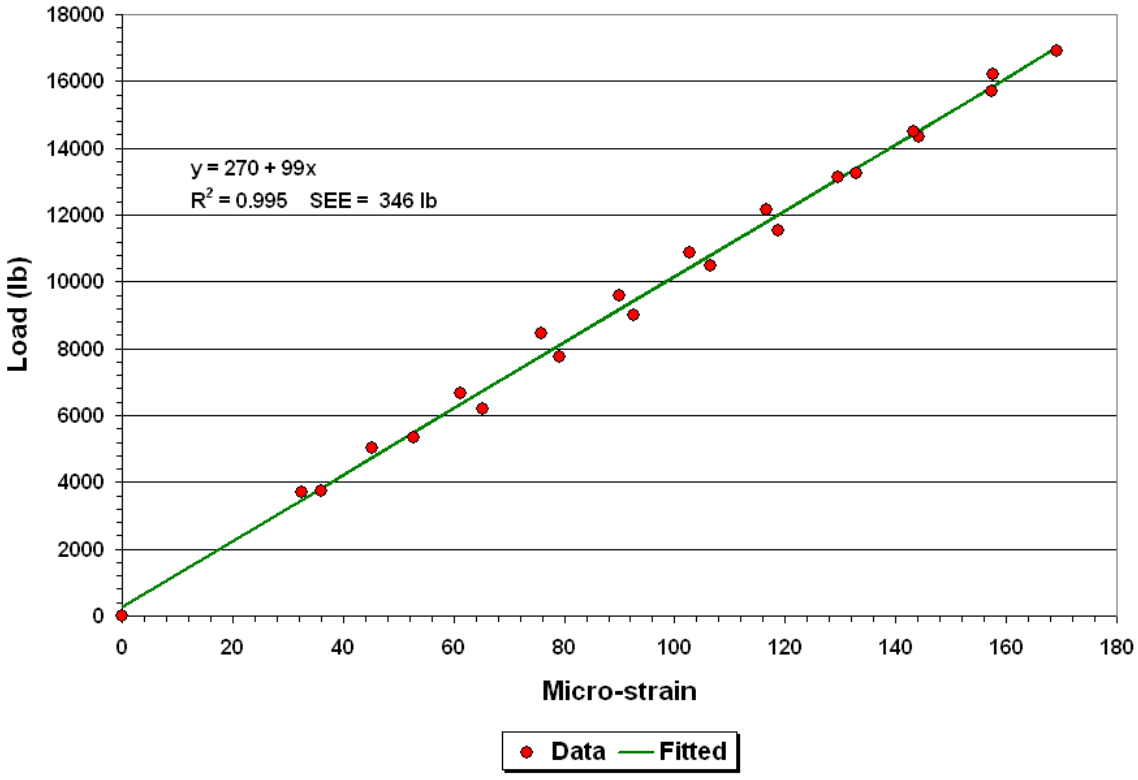

Figure 2.25. Strain Gage Calibration Curve for Right Side of Trailer Lead Axle.

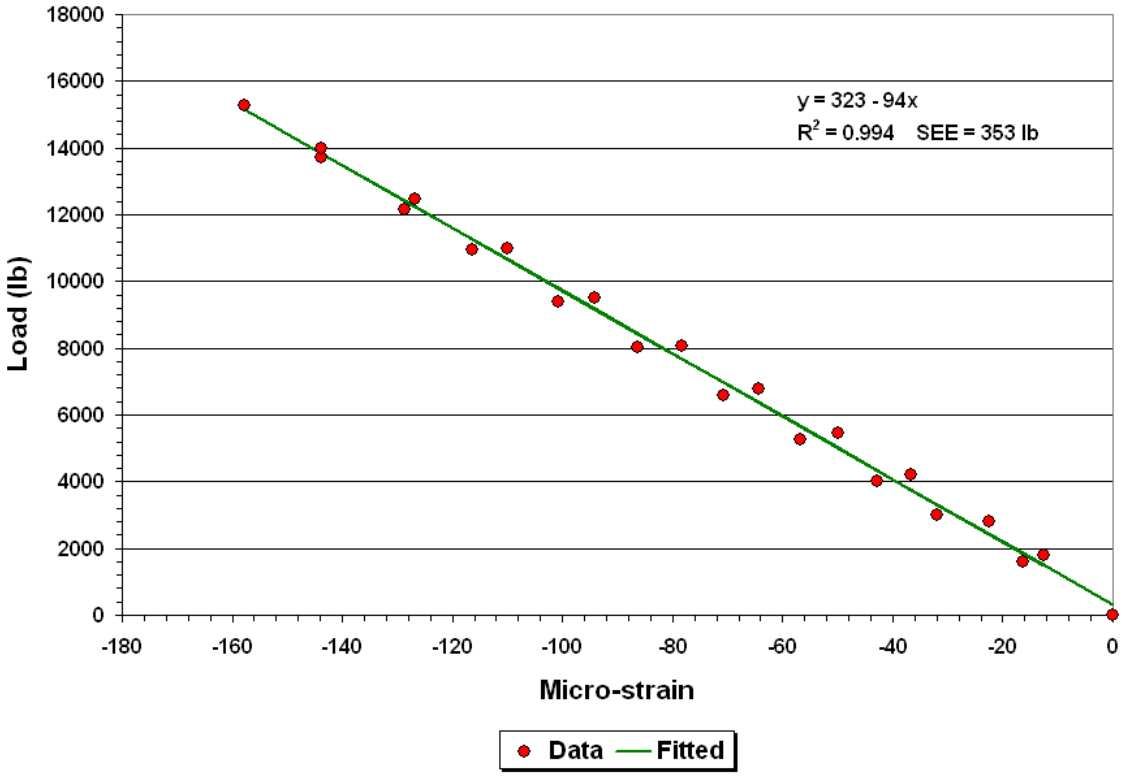

Figure 2.26. Strain Gage Calibration Curve for Left Side of Second Trailer Axle.

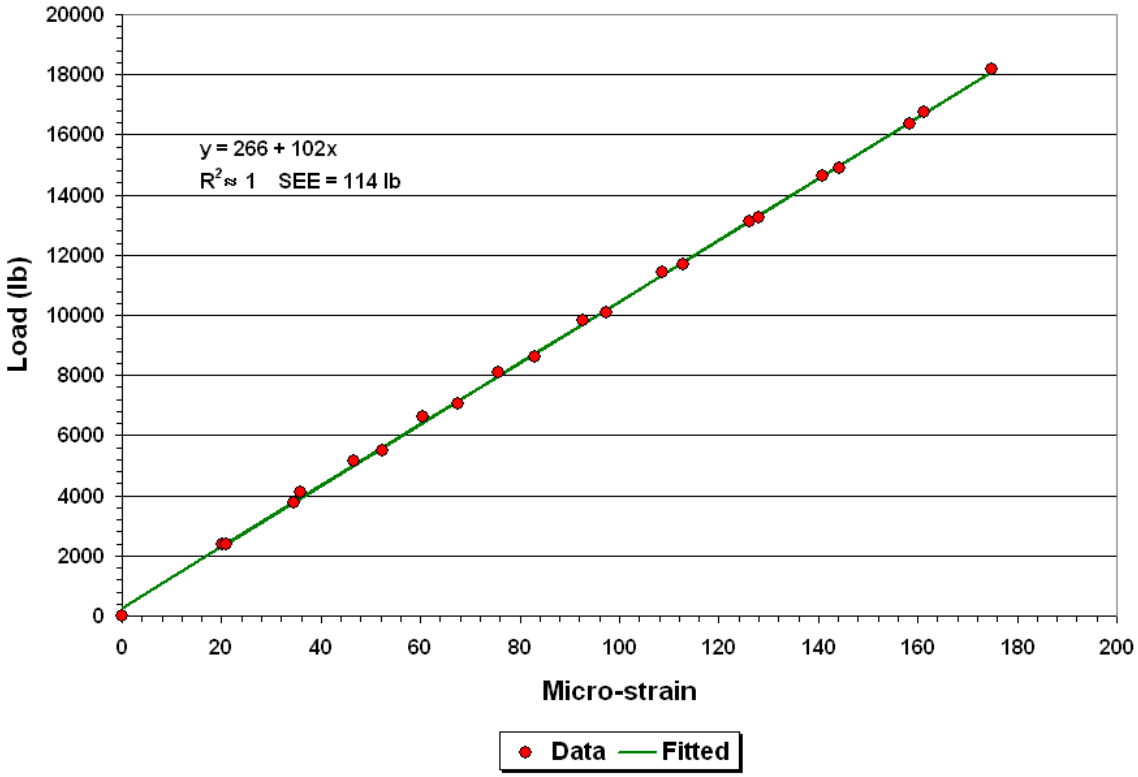

Figure 2.27. Strain Gage Calibration Curve for Right Side of Second Trailer Axle.

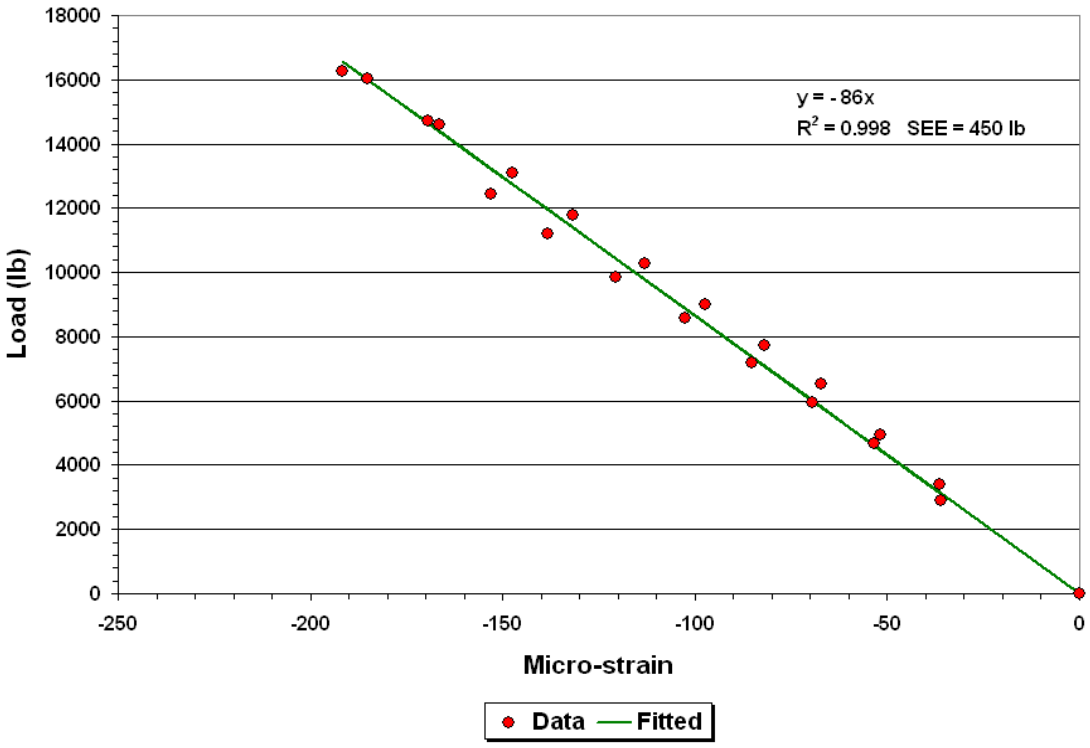

Figure 2.28. Strain Gage Calibration Curve for Left Side of Drive Lead Axle.

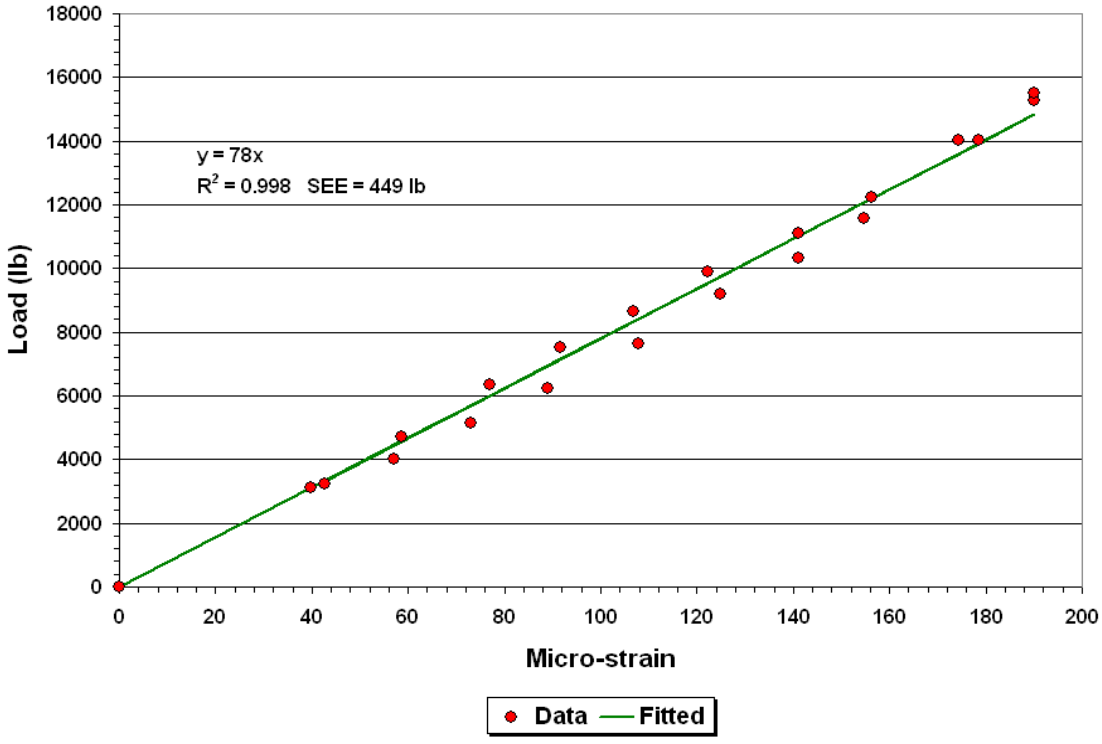

Figure 2.29. Strain Gage Calibration Curve for Right Side of Drive Lead Axle.

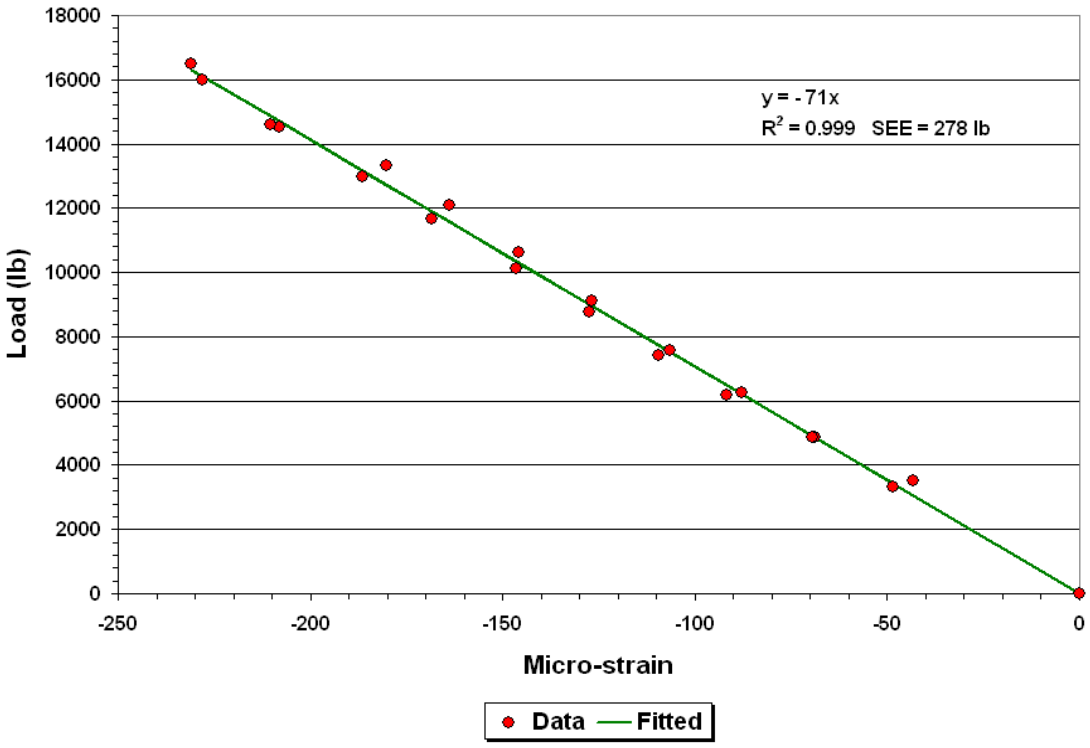

Figure 2.30. Strain Gage Calibration Curve for Left Side of Drive Trailing Axle.

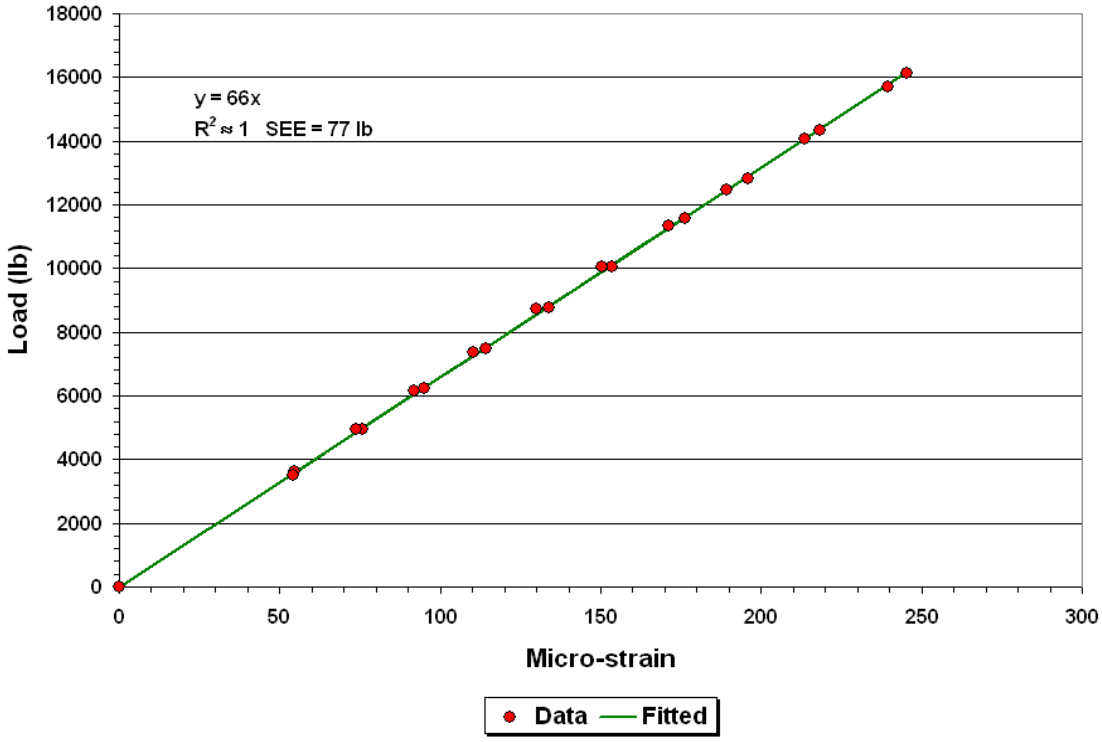

Figure 2.31. Strain Gage Calibration Curve for Right Side of Drive Trailing Axle.

Figures 2.32 and 2.33 show the calibration relationships determined for the steering axle strain gages. During calibration, researchers observed that the tire loads on the steering

axle did not vary appreciably with changes in the load applied through the drive axle assembly, as may be inferred from the range of tire loads plotted in Figures 2.32 and 2.33. This observation is consistent with weigh-in-motion data on five axle tractor-semitrailer combination trucks where the most consistent axle weight is from the steer axles, which remains reasonably constant under various loading scenarios.

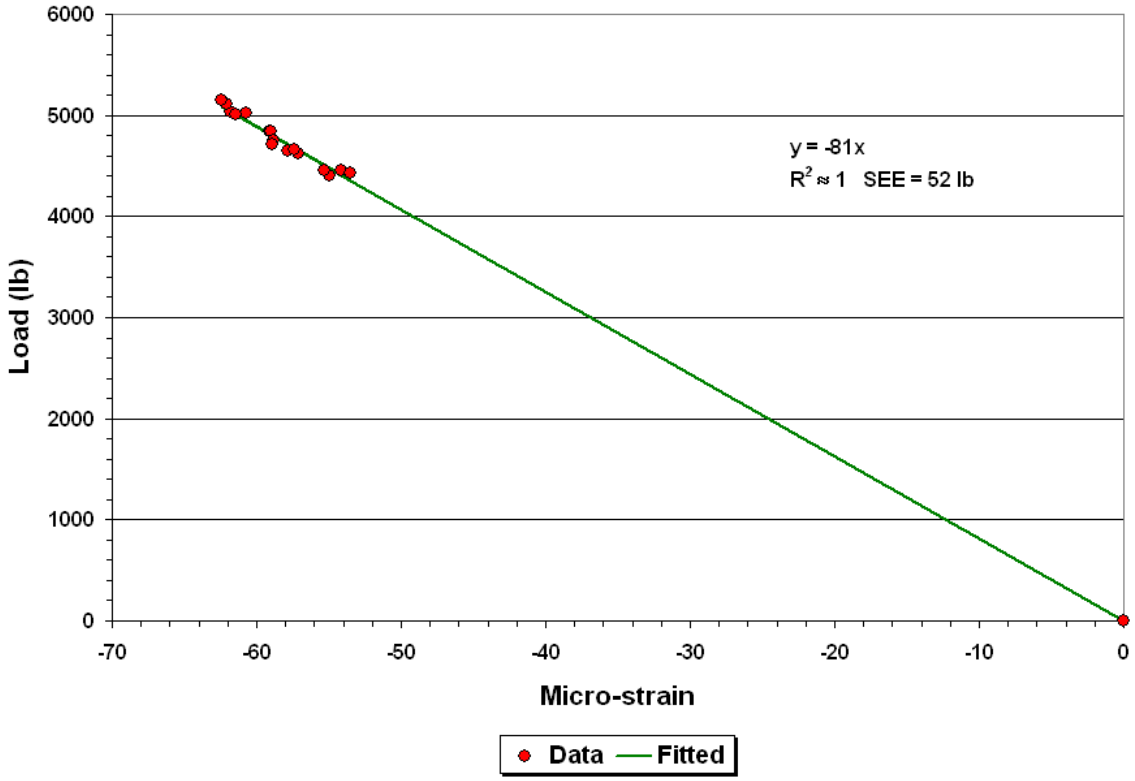

Figure 2.32. Strain Gage Calibration Curve for Left Side of Steering Axle.

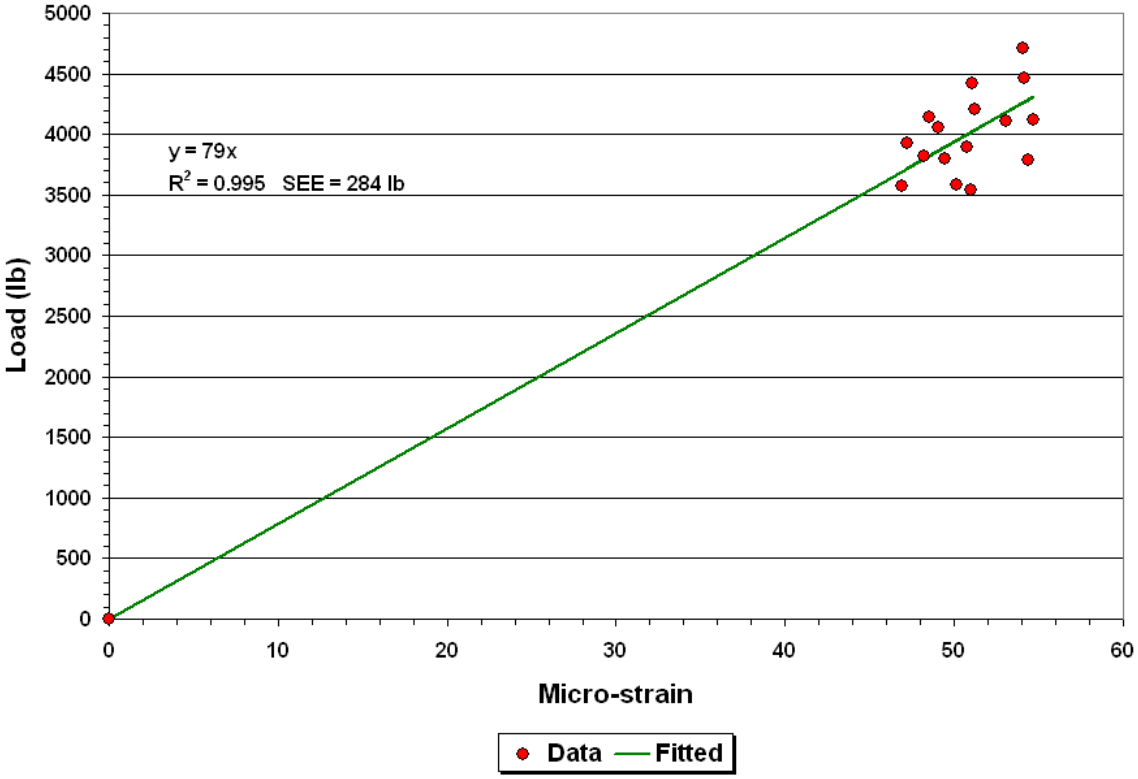

Figure 2.33. Strain Gage Calibration Curve for Right Side of Steering Axle.

CHAPTER III. FABRICATION AND VERIFICATION OF INERTIAL PROFILING SYSTEM

Profile measurements are needed to evaluate relationships between vehicle dynamic loads and surface roughness for the purpose of evaluating the current ride specification in this project. Initially, researchers instrumented a tractor-semitrailer with a portable inertial profiling system to permit synchronized collection of dynamic tire loads and surface profiles during testing. However, tests to verify profiler performance based on the certification requirements in TxDOT Test Method Tex-1001S were not successful. Compared to the vibrations from vans or light trucks on which profilers are commonly used, the vibrations from the test vehicle were considerably larger, resulting in failure of the dampeners used to isolate the accelerometers and lasers of the profiling system from vibrations of the test vehicle during testing. The dampeners sheared off after several repeat runs of the test truck on the pavement sections used to evaluate the on-board inertial profiling system.

Following the suggestion of the project monitoring committee, researchers dropped the idea of instrumenting a tractor-semitrailer with an inertial profiling system. Instead of this approach, profile data were to be collected using a high-speed inertial profiler separate from the instrumented vehicle combination. To minimize differences between wheel paths tracked, the sensors of the inertial profiler would be set to match the spacing between the dual wheels on the left and right sides of the instrumented tractor-semitrailer. In addition, the operator of the inertial profiler would try to take data as close as possible on the same wheel paths where dynamic load measurements were collected with the instrumented truck.

Ordinarily, this project would have used one of TxDOT's inertial profilers to collect profile measurements. However, problems with the availability of an inertial profiler led researchers to instrument a test vehicle with an inertial profiling system to conduct the required tests. This instrumentation was an in-house effort funded by TTI. The profiling system followed the same design developed by Walker (1997) and used existing software. The main components of the profiler are:

- a chassis unit containing the power supply and signal interface modules,
- two laser/accelerometer modules mounted on the front of the test vehicle,
- a Model 9803 Data Translation board for data acquisition,
- a distance encoder,

- a start sensor, and
- a notebook computer.

Figure 3.1 shows the laser/accelerometer modules mounted in front of the TTI truck that researchers instrumented for inertial profile measurements. As shown, the modules are positioned on a bar that goes into receiver hitches located on the front bumper of the truck. The groove along the middle of the bar permits the operator to position each module along the bar and vary the sensor spacing. The modules are tightened in place by set screws. In addition, the height of the bar can be changed to accommodate lasers with different standoffs.

Researchers evaluated the profiler shown in Figure 3.1 on the certification pad located at the Riverside Campus of Texas A&M University. For this evaluation, data were taken along the left and right wheel paths of two 530-ft sections (one smooth and the other medium-smooth) that researchers selected for testing the inertial profiler. Runs were made in the northbound direction of the pad, and profile elevations were recorded at 0.96-inch intervals in the data files. A total of 20 runs were made, 10 on each section. Researchers analyzed the test data to evaluate profile repeatability and accuracy, as well as IRI repeatability and accuracy.

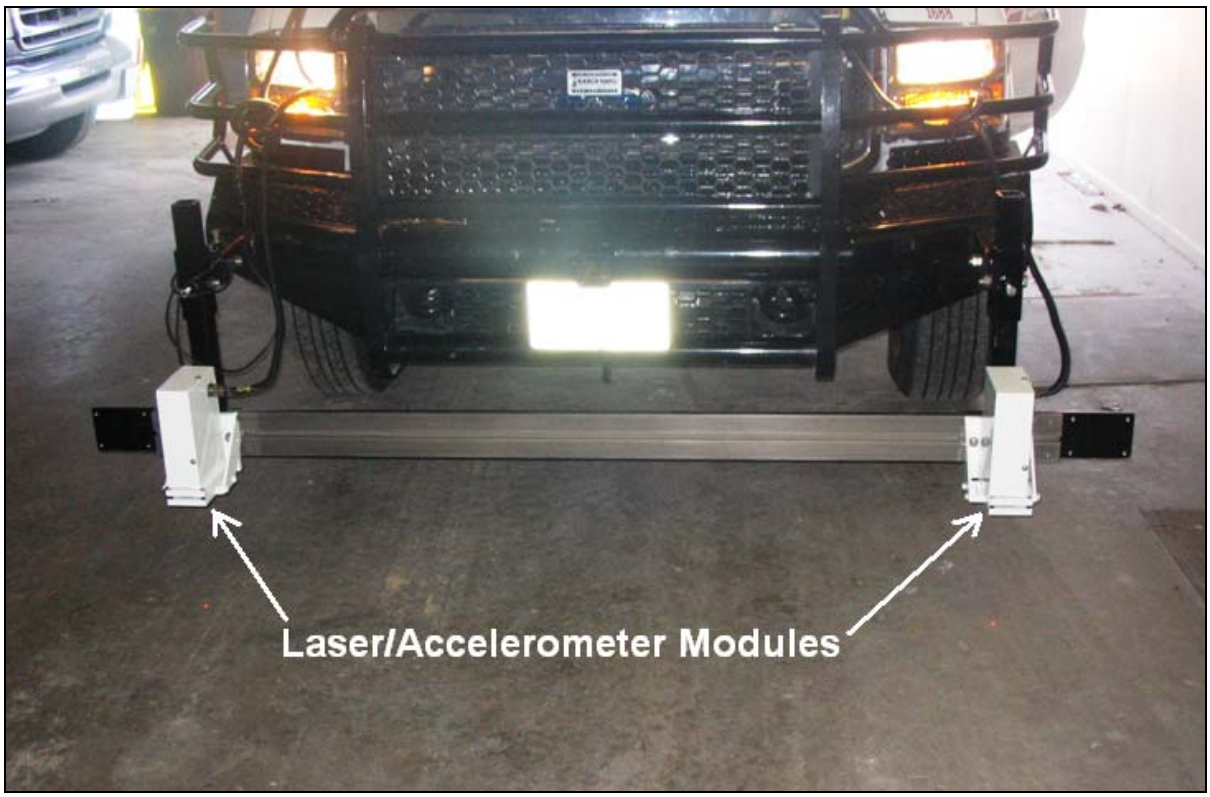

Figure 3.1. Laser/Accelerometer Modules Mounted in Front of Test Vehicle.

Figures 3.2 to 3.5 illustrate the repeatability of the profiles measured on each section. Tables 3.1 to 3.4 summarize the statistics determined from the analysis of test data. The results presented show that the profiler (as configured) meets the requirements for inertial profiler certification stipulated in TxDOT Test Method Tex-1001S and that a suitable profiling system has been built for use on this project as well as on other research projects where this capability is needed.

Having successfully fabricated an inertial profiler, researchers collected profile data on a number of TxDOT paving projects to evaluate the Department's current Item 585 ride specification. Table 3.5 identifies the projects tested. All projects, with the exception of SH47 in Brazos County, were completed within 3 months of the profile surveys done in this research project. SH47 is an existing highway that is not a newly resurfaced project. Researchers included SH47 on the routes that were surveyed because of the smooth ride scores reported on this highway in TxDOT's pavement management information system database. On the same projects identified in Table 3.5, researchers collected dynamic tire load data using the instrumented tractor-semitrailer combination described in Chapter II of this interim report. Researchers then analyzed these measurements in conjunction with the profile data collected on these projects to evaluate TxDOT's Item 585 ride specification. The reader is referred to the final project report by Fernando, Harrison, and Hilbrich (2007) for the details of this evaluation.

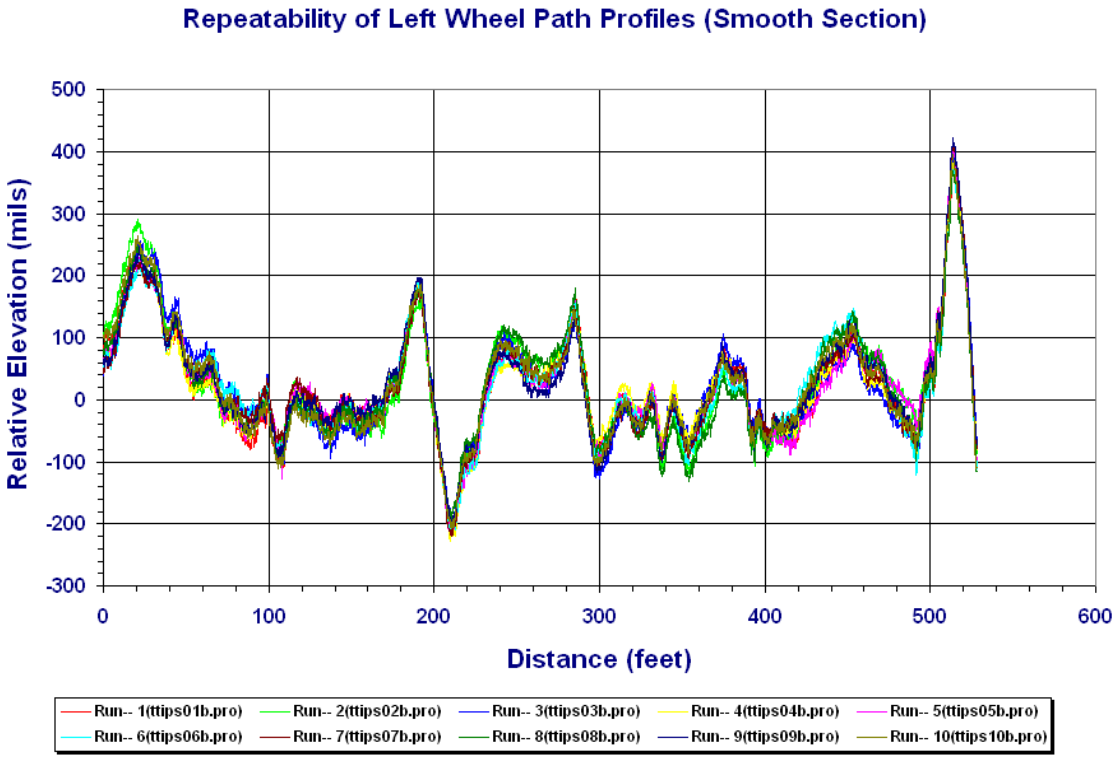

Figure 3.2. Repeatability of Profiles Measured on Left Wheel Path of Smooth Section.

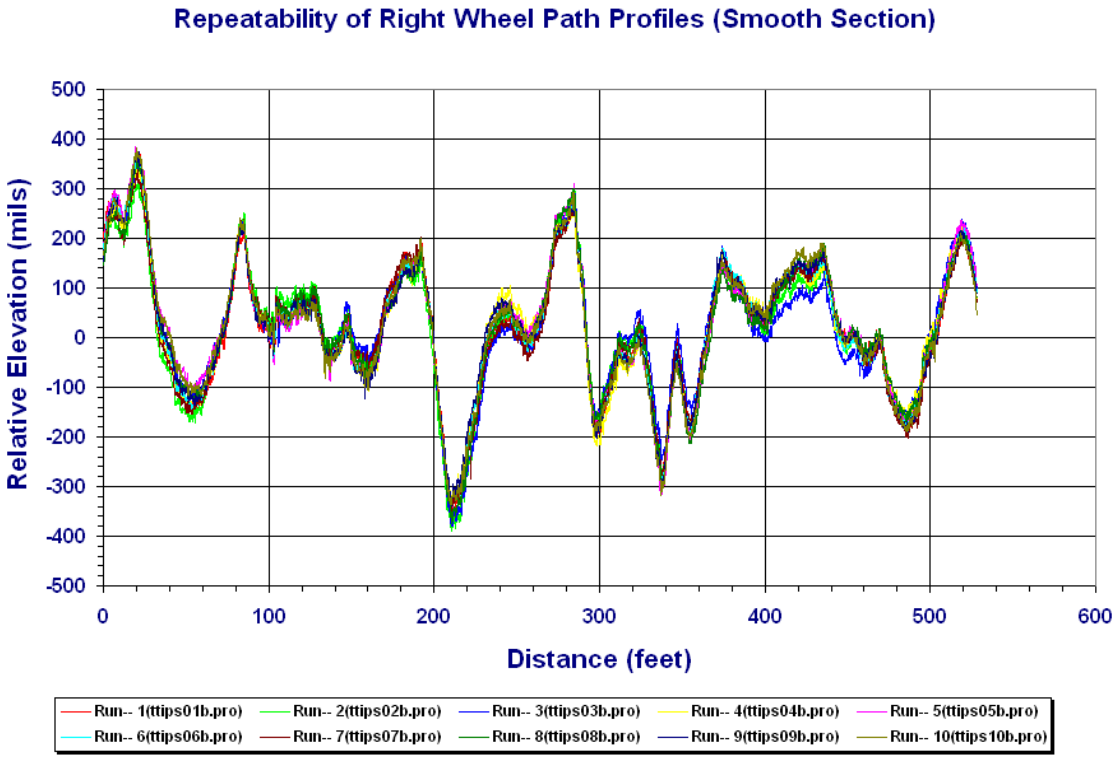

Figure 3.3. Repeatability of Profiles Measured on Right Wheel Path of Smooth Section.

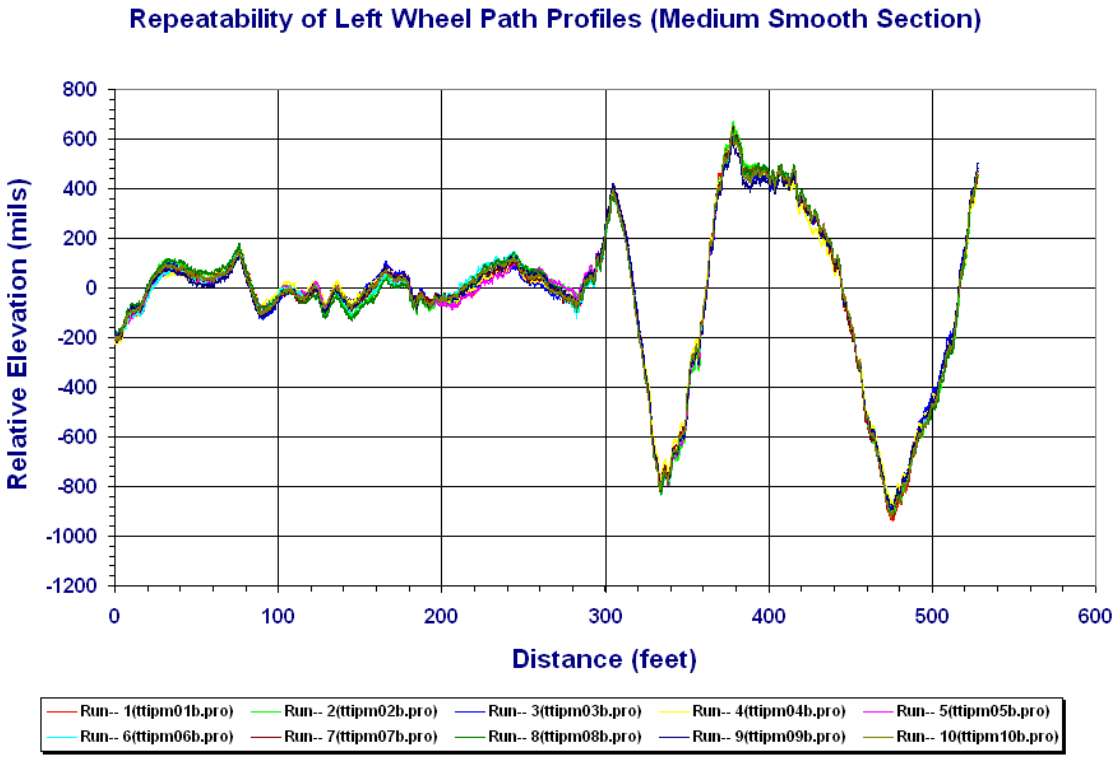

Figure 3.4. Repeatability of Profiles Measured on Left Wheel Path of Medium Smooth Section.

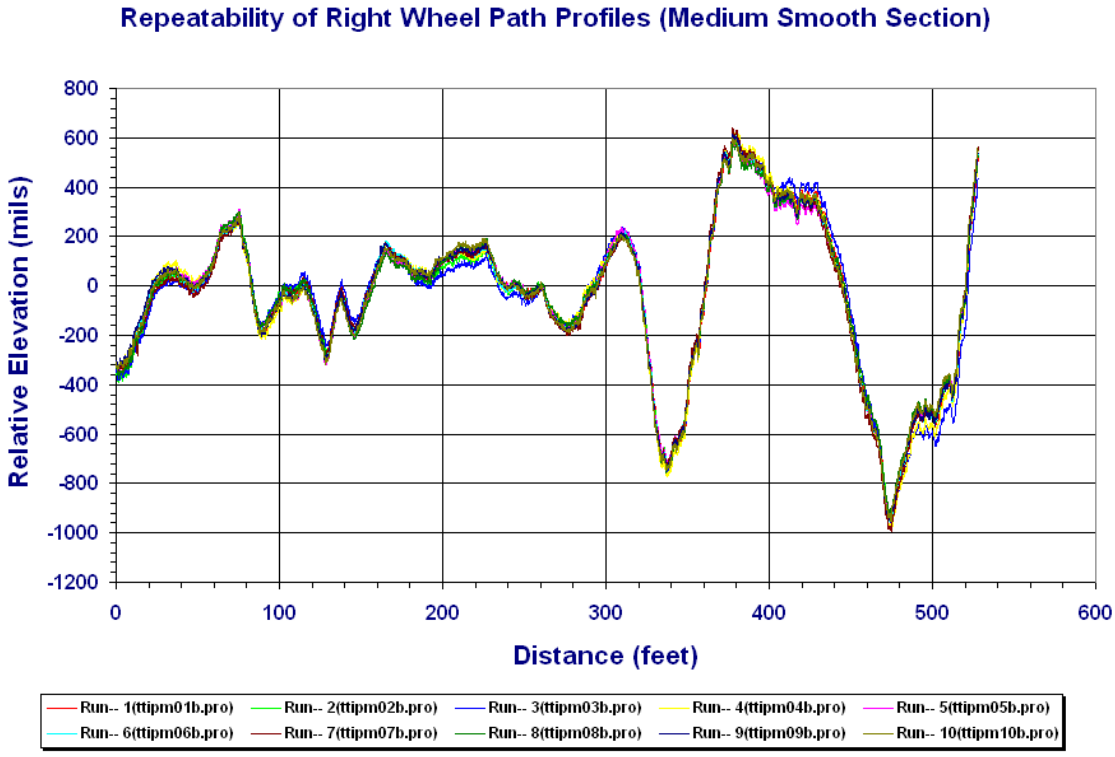

Figure 3.5. Repeatability of Profiles Measured on Right Wheel Path of Medium Smooth Section.

Table 3.1. Repeatability of Profile Measurements from TTI Profiler.

Test Section	Wheel Path	Average Standard Deviation (mils)[1]
Smooth	Left	16
	Right	17
Medium-Smooth	Left	18
	Right	21

[1] Not to exceed 35 mils per TxDOT Test Method Tex-1001S

Table 3.2. Repeatability of IRIs from Profile Measurements with TTI Profiler.

Test Section	Wheel Path	Standard Deviation (inches/mile)[1]
Smooth	Left	0.89
	Right	0.74
Medium-Smooth	Left	1.10
	Right	0.54

[1] Not to exceed 3.0 inches/mile per TxDOT Test Method Tex-1001S

Table 3.3. Accuracy of Profile Measurements from TTI Profiler.

Test Section	Wheel Path	Average Difference (mils)[1]	Average Absolute Difference (mils)[2]
Smooth	Left	-1	11
	Right	0	11
Medium-Smooth	Left	2	13
	Right	3	13

[1] Must be within ±20 mils per TxDOT Test Method Tex-1001S
[2] Not to exceed 60 mils per TxDOT Test Method Tex-1001S

Table 3.4. Accuracy of IRIs from Profile Measurements with TTI Profiler.

Test Section	Wheel Path	Difference (inches/mile)[1]
Smooth	Left	0.12
	Right	0.94
Medium-Smooth	Left	0.04
	Right	-1.19

[1] Absolute difference not to exceed 12 inches/mile per TxDOT Test Method Tex-1001S

Table 3.5. Highways Where Researchers Collected Profile and Dynamic Load Measurements.

Highway	County	Pavement Type	Limits		Number of Lanes	Length (miles)
			From	To		
SH21	Lee	Asphalt concrete	Jct. with US77	2.7 miles east of US77	4	2.4
SH21	Bastrop	Asphalt concrete	Jct. with US290	2.8 miles east of FM1441	4	3.6
SH47	Brazos	Asphalt concrete	RM412	RM418	2	6.0
SH47	Brazos	Asphalt concrete	RM418	5.7 miles from RM418	2	5.7
FM102 Group A	Wharton	Asphalt concrete	Wharton County Line	FM102 highway sign	2	5.0
FM102 Group B	Wharton	Asphalt concrete	RM504	RM510	2	6.0
SH36	Fort Bend	Asphalt concrete	Jct. with FM1994	Jct. with FM442	2	1.4
FM1462	Fort Bend	Asphalt concrete	Jct. with SH36	Jct. with FM361	2	3.6
FM1994	Fort Bend	Asphalt concrete	Jct. with SH36	Jct. with FM361	2	2.0
SH121 Group A	Denton	Portland cement concrete	Jct. with Hebron Parkway	Jct. with IH35	2	2.0
SH121 Group B	Denton	Portland cement concrete	Light pole at IH35 jct.	FM544 exit ¼ mile sign	2	2.3
SH121 Group C	Denton	Portland cement concrete	Sign post for IH35E N. Denton exit only	Jct. with IH35	2	1.18
SH121 Group D	Denton	Portland cement concrete	Jct. with IH35	Jct. with Denton Tap Road	1	2.26

CHAPTER IV. SUMMARY OF FINDINGS

This interim report documented the research efforts conducted in this project to provide an instrumented tractor-semitrailer combination for measurement of dynamic loads, and a high-speed inertial profiler for measurement of surface profiles. These capabilities are needed to collect data with which to evaluate TxDOT's Item 585 smoothness specification for the purpose of verifying whether it permits certain profile wavelengths to pass that are detrimental to pavement life based on dynamic loading criteria. Based on the experience with the instrumentation efforts, the authors note the following findings:

- The application of strain gages for load measurement was successfully demonstrated in a laboratory setting with a shear beam load cell experiment wherein a steel bar, instrumented with shear strain gages in a full bridge configuration, was used to measure the total weight of a known set of circular disks. The shear beam load cell gave a measurement within 0.33 percent of the known total weight of the circular disks.
- Small-scale testing with an instrumented trailer verified the method for positioning, mounting, wiring, and calibrating the strain gages on the test vehicle. From the results of the trailer calibration, researchers observed a strong linear relationship between tire load and strain over the range of loads at which the calibration was conducted. In addition, results of tests on a weigh-in-motion site showed that:
  - the dynamic tire loads determined from the strain gages vary closely about the measured static tire load of 700 lb,
  - the dynamic tire loads determined around the vicinity of the WIM sensor are in reasonable agreement with the corresponding WIM measurement on each repeat run, and
  - the load measurements exhibit similar patterns between repeat runs.

  In view of the positive results, researchers proceeded with instrumenting and calibrating a tractor-semitrailer combination following the same approach used for the small-scale trailer tests.
- The calibration curves from full-scale laboratory tests of the instrumented tractor-semitrailer exhibit a strong linear relationship between tire load and shear strain. The

shear strains measured between the left and right sides of a given axle also show a difference in signs, as expected from theory.

- Researchers also instrumented a test vehicle with an inertial profiling system and verified its performance based on TxDOT Test Method Tex-1001S. The results obtained show that the profiler meets the certification requirements specified in the test method.

REFERENCES

Addis, R. R., A. R. Halliday, and C. G. B. Mitchell. Dynamic Loading of Road Pavements by Heavy Goods Vehicles. Congress on Engineering Design, Seminar 4A-03, Birmingham, Institution of Mechanical Engineers, 1986.

Chatti, K., and D. Lee. Development of New Profile-Based Truck Dynamic Load Index. *Transportation Research Record 1806*, Transportation Research Board, Washington, D.C., 2002, pp. 149-159.

Dally, J. W., and W. F. Riley. *Experimental Stress Analysis*. 2nd edition, McGraw-Hill, Inc., N.Y., 1978.

Fernando, E. G., G. Harrison, and S. Hilbrich. Evaluation of Ride Specification Based on Dynamic Load Measurements from Instrumented Truck. Technical Report 0-4863-2, Texas Transportation Institute, Texas A&M University, College Station, Tex., 2007.

Fernando, E. G. Index for Evaluating Initial Overlay Smoothness with Measured Profiles. *Transportation Research Record 1806*, Transportation Research Board, Washington, D.C., 2002, pp. 121-130.

Fernando, E. G., and C. Bertrand. Application of Profile Data to Detect Localized Roughness. *Transportation Research Record 1813*, Transportation Research Board, Washington, D.C., 2002, pp. 55-61.

Fernando, E. G. Development of a Profile-Based Smoothness Specification for Asphalt Concrete Overlays. Research Report 1378-S, Texas Transportation Institute, Texas A&M University, College Station, Tex., 1998.

Gyenes, L., and C. G. B. Mitchell. Measuring Dynamic Loads for Heavy Vehicle Suspensions Using a Road Simulator. *International Journal of Heavy Vehicle Systems*, Vol. 3, 1996.

Hassan, R. A., and K. McManus. Assesssment of Interaction Between Road Roughness and Heavy Vehicles. *Transportation Research Record 1819*, Transportation Research Board, Washington, D.C., 2003, pp. 236-243.

Huhtala, M., V. Laitinen, and P. Halonen. Roughness Measurement Devices and Dynamic Truck Index. International Conference on the Bearing Capacity of Roads and Airfields, Minneapolis, Minn., 1994, pp. 1517-1531.

Jacob, B., and V. Dolcemascolo. Dynamic Interactions Between Instrumented Vehicles and Pavements. International Symposium on Heavy Vehicle Weights and Dimensions, Queensland, Australia, 1998, pp. 142-160.

Merril, D. B., D. Blackman, and V. Ramdas. The Implications of Dynamic Loading and Tire Type on the UK Road Network. International Conference on Asphalt Pavements, Copenhagen, Denmark, 2002.

Middleton, J., and A. H. Rhodes. The Effect of Dynamic Loading on Road Pavement Wear: A Study of the Relationship Between Road Profiles and Pavement Wear on an Instrumented Test Road. *Proceedings of the Institution of Civil Engineers*, Vol. 105, 1994.

Papagiannakis, T., and B. Raveendran. International Standards Organization – Compatible Index for Pavement Roughness. *Transportation Research Record 1643*, Transportation Research Board, Washington, D.C., 1998, pp. 110-115.

Roberts, F. L., J. T. Tielking, D. Middleton, R. L. Lytton, and K. Tseng. Effects of Tire Pressures on Flexible Pavements. Research Report 372-1F, Texas Transportation Institute, Texas A&M University, College Station, Tex., 1986.

Steven, B., and J. de Pont. Dynamic Loading Effects on Pavement Performance – The OECD Divine Test at CAPTIF. ARRB Transport Research Conference, Christchurch, New Zealand, 1998, pp. 93-107.

University of Michigan Transportation Research Institute (UMTRI). RoadRuf User Reference Manual, The University of Michigan, Ann Arbor, Mich., 1997.

Walker, R. S. Real-Time Data Acquisition for Surface Measurement/Implementation of Intelligent Bus Systems for Distress Measurements. Research Report 19987-F, The University of Texas at Arlington, Arlington, Tex., 1997.

Wang, F., and R. B. Machemehl. Current Status and Variability of In-Service Truck Tire Pressures in Texas. *Transportation Research Record 1853*, Transportation Research Board, Washington, D.C., 2003, pp. 157-164.

Wang, F., R. F. Inman, R. B. Machemehl, Z. Zhang, and C. M. Walton. Study of Current Truck Configurations. CTR Report 0-1862-1, Center for Transportation Research, The University of Texas at Austin, Austin, Tex., 2000.

APPENDIX
LITERATURE REVIEW

Researchers conducted a literature review to gather information considered useful for accomplishing the objectives of this project. The review covered the following areas:

- measurement of vehicle dynamic loads,
- surveys of truck use that identified configurations commonly used by carriers to transport goods and commodities,
- profile statistics for characterizing pavement smoothness based on truck damage criteria,
- vehicle transfer functions relating pavement roughness to dynamic tire loading, and
- compilations of data on truck properties for simulating the response of trucks to pavement roughness.

The findings from the literature review are presented in this appendix.

TRUCK TESTS TO INVESTIGATE RELATIONSHIPS BETWEEN PAVEMENT ROUGHNESS, VEHICLE CHARACTERISTICS, AND DYNAMIC TIRE LOADS

In a 1996 report, Gyenes and Mitchell detail research conducted at Transport Research Laboratories (TRL) in the United Kingdom (UK), in which the Volvo test facility in Gothenburg was utilized to develop a simulated test to rate suspensions in terms of their potential for causing road wear. This goal was accomplished by comparing simulated wheel load measurements published by TRL in 1993 to actual dynamic behavior of heavy goods vehicle suspensions over the TRL test track. The first test series in 1991 involved a computer-controlled Volvo rig made up of six hydraulic actuators capable of exercising a fully laden vehicle. The TRL test track profiles were run through the actuators, and a comparison was made between the Volvo instrumentation, which measured the dynamic loads under the tire patch using load cells built into the actuators, and the TRL instrumentation, which used strain gages and accelerometers. In addition, researchers compared rig generated wheel load histories against real road-based load histories from the TRL test track program.

A second test series was conducted in 1993 to obtain the unsprung masses by the process of dynamic calibration, followed by systematic runs at simulated test speeds of 20,

30, 40, 50, and 60 mph using the smooth and medium-smooth wheel track profiles of the TRL test track as inputs. The suspensions for the two-axle semitrailer bogies used for testing included a tandem axle air suspension; a tandem axle, single-leaf steel suspension; and a rubber mounted walking beam suspension. The vehicles were fully loaded to the UK gross vehicle weight limit of 32.5 tons with tandem axle weights of about 18 tons on each semitrailer bogie.

Wheel loads on the road simulator were measured using load cells built into the actuators close to the wheel platforms. The load on each wheel of the replaceable sub-chassis unit was determined by measuring the bending of the axle between the spring mount and the wheel hub using strain gages, and the vertical inertia of the wheel mass using an accelerometer mounted on the hub back plate. Strain gages fitted to the bogie with the rubber-mounted walking beam suspension measured the shear force on the axle tube, a technique that provided higher accuracy in dynamic load measurement compared to bending gages.

Accelerometers were fitted to the semitrailer platform to measure body bounce, pitch, and roll accelerations. Displacement transducers were also fitted to each semitrailer wheel to measure vertical displacement between the axle center and the trailer platform. The accelerometers and strain gages were calibrated before each test series, and the signals from the actuator sensors and body-mounted sensors were recorded on the same data logger. The steel, air, and rubber-suspended tandem axles were sinusoidally excited over a range of frequencies from 0.5 Hz to 20 Hz in bounce, pitch, roll, and twist modes. The results of the constant speed excitation in bounce for the nearside rear wheel of all three suspension types indicate that there are two dominant modes – the body bounce at low frequency and the wheel hop at high frequency. As the excitation frequency is increased, the effect of the unsprung mass on wheel loads becomes significant. The results of the constant speed excitation in pitch for the nearside rear wheel of all three suspension types indicate that there is one dominant mode, which is at high frequency. The results of the constant speed excitation in roll for the nearside rear wheel of all three suspension types are evident at around 1 Hz. The results of the constant speed excitation in twist for the nearside rear wheel of all three suspension types indicate that there is no distinct mode in the range of excitation frequencies.

The results of these tests showed that the dynamic wheel load can be measured within 1 to 2 percent accuracy when using an improved technique, which involves the use of shear gages and a dynamic calibration procedure that corrects for the angular and vertical accelerations of the wheel components outboard of the strain gages. According to the researchers, this method is an improvement over other methods, which use bending gages that are subject to anomalous readings of the roll component of wheel load.

Middleton and Rhodes' 1994 report detail their research, which was based on previous work conducted by Addis, Halliday, and Mitchell in 1986. In the research performed by Addis et al., a two-axle, semitrailer was instrumented, and results were obtained from one vehicle operating over one instrumented pavement. Middleton and Rhodes decided to further this research and constructed a test laboratory with a more comprehensive system of strain gages that could be used to monitor the structural effects of the passage of any vehicle passing over the test section at various speeds. Each strain gage was calibrated using dynamic wheel loads data from an instrumented two-axle heavy goods vehicle, which allowed the monitoring of instantaneous dynamic wheel loads of any vehicle at any point along the test section. The test facility was instrumented with strain gages with 120 ohm resistance-foil located at the bottom of the roadbed to measure the transient horizontal radial strain at 0.5 m centers under each wheel path. There were a total of 126 strain gages.

The test vehicle used in the study was a Volvo instrumented at TRL. It was instrumented to permit measurements of all wheel loads simultaneously, using strain gages that measured the bending of the axles between the suspension and the hub. Accelerometers were also used to correct the vertical inertial loads due to the unsprung mass outboard of the strain gages.

The instrumented test vehicle was used to calibrate the strain gages. This was done to establish the relationship between vehicle speed, transient strain, and the respective dynamic wheel loads. The calibration data were used so that the instantaneous wheel loads of any vehicle traveling along the wheel paths could be monitored.

The longitudinal profiles of the two wheel-tracks were monitored regularly using the TRL high speed road monitor. During testing, a record was kept for temperature, wind speed, and rainfall in order to ensure that strain measurements were taken under similar conditions. Wheel paths were surveyed regularly for rutting and cracking. Twelve sets of

dynamic wheel load data were collected under a combination of variables, which included number of axles, speed, and number of wheel paths. A minimum of two sets of pavement strain data were collected for each strain gage, and thermocouples were used to measure the pavement temperatures at the surface, at 20 mm depth, and at 250 mm depth at the beginning, middle, and end of the test section.

The results of this research provided several conclusions. One conclusion was that the wheels of the test vehicles applied dynamic loading, which oscillated between 3 Hz and appeared to be independent of speed, load, tire type, and suspension system. Also, the researchers concluded that each axle of the test vehicles applied maximum and minimum dynamic loads at common points for a specific speed and that the ratio of mean dynamic axle load and static axle load increased with speed.

Jacob and Dolcemascolo's 1998 report details their investigation into dynamic loads on pavements and their spatial repeatability to assess the sensitivity to pavement profile, road roughness, vehicle characteristics, and traveling conditions. The investigation also looked into the effects of dynamic loads on vehicles and the infrastructure and focused on the response of two instrumented vehicles traveling at the same speeds on different road profiles, whose evenness were considered excellent, good, and poor. The IRI values in m/km of each road section were found to be 0.8 for the road in excellent condition, 1.73 for the road in good condition, and 3.57 for the road in poor condition.

The two vehicles were instrumented with strain gages mounted on the axles and accelerometers on the bodies, which provide the data to calculate dynamic wheel impact forces at high frequency. The wheel load instrumentation was made up of two strain gage bridges and two accelerometers per axle, which were configured as full bridge circuits that were sensitive to shear force. These instrumented vehicles could measure dynamic wheel loads with a sampling frequency of 500 Hz.

An instrumented vehicle was also used in this research, which consisted of a two-axle tractor with a single-axle instrumented trailer that could be equipped with two suspension types, which were either air or steel leaf spring. This instrumented vehicle could measure dynamic wheel loads with a sampling frequency of 200 Hz.

For each of the three test sites, the power spectral density (PSD) of the pavement profile was calculated and plotted versus the wavelength λ. The PSD may be plotted as a function of frequency f or wavelength because both are linked to the vehicle velocity V

according to the relation $V = f \lambda$. When plotting the PSD of the pavement profile, the larger the area under the PSD curve, the greater the roughness.

Two PSDs were calculated for the impact forces of the trailer corresponding to each combination of the test variables, i.e., test site, suspension, load, and speed. One PSD was for the axle impact force, which is the sum of both wheel loads and is considered to be representative of the bounce and axle hop motions. The other PSD was for the difference between the left and right wheel loads, which is representative of the roll motion. The main findings were that the body bounce of the steel suspension gives the highest peaks, which generally increased with pavement roughness. The body bounce peak amplitude is between 10 to 20 times lower with the air suspension than with the steel suspension.

PSDs were also calculated for each wheel and axle load of the instrumented vehicle. It was found that the shapes of the PSDs for wheel and axle loads are similar for each speed with the same approximate peaks. The roll effect is more important for wheels, while the axle hop is higher for axles. The body motions were dominant for the heaviest load, while the axle hops became the main effect at lower loads with a slight shift in the frequency. Other significant findings of this research were the importance of wheel imbalance to the wheel and axle dynamic impact factors (especially at low speed and on smooth road profiles where the body bounce and axle hop motions are low), the significant reduction in dynamic load increments from the air suspensions, and the great influence of pavement roughness on dynamic loads.

INDICES CHARACTERIZING TRUCK DYNAMIC LOADING

The effect of surface profile on vehicle dynamic loads is illustrated in Figures A1 to A3 (Fernando, 2002). Shown in these figures are the predicted vehicle responses to measured surface profiles as determined using a vehicle simulation model. Figure A1 shows the predicted variation in dynamic axle loads on a smooth pavement having a serviceability index (SI) of 4.5. The plot shown is referred to in this proposal as the dynamic load profile, analogous to a surface or road profile, which shows the variation in elevation with distance along a given segment. Figure A2 illustrates the predicted dynamic load profile for a medium-smooth pavement (SI of 3.4), while Figure A3 shows the load profile for a rough pavement (SI of 2.5). It is observed from Figures A1 to A3 that the variability in predicted dynamic axle loads increases with an increase in surface roughness.

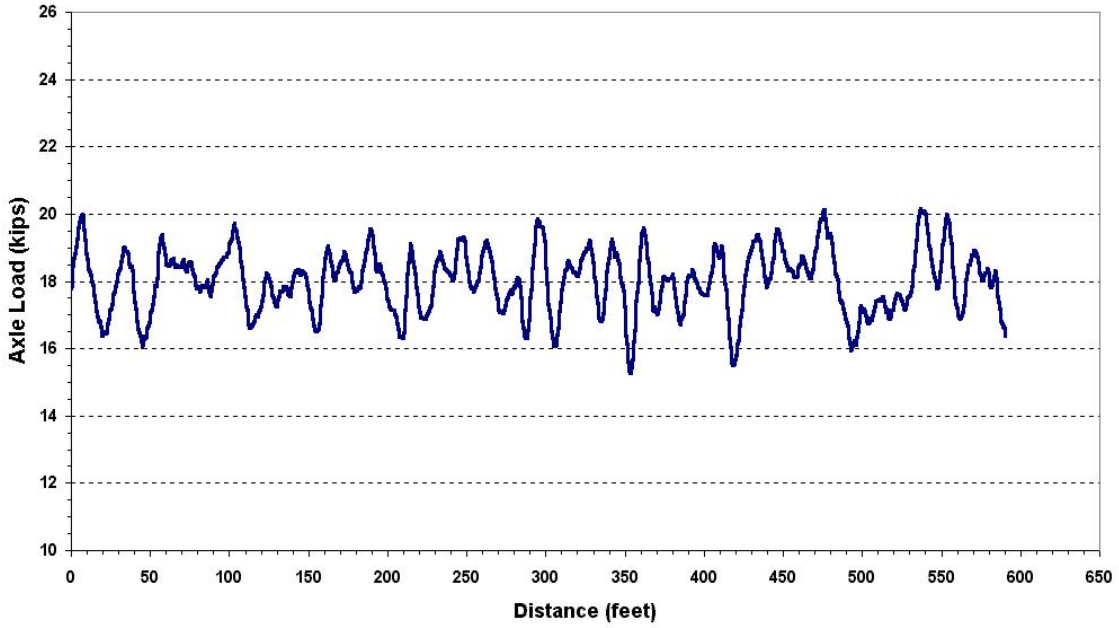

Figure A1. Predicted Dynamic Loads on a Smooth Pavement (SI = 4.5).

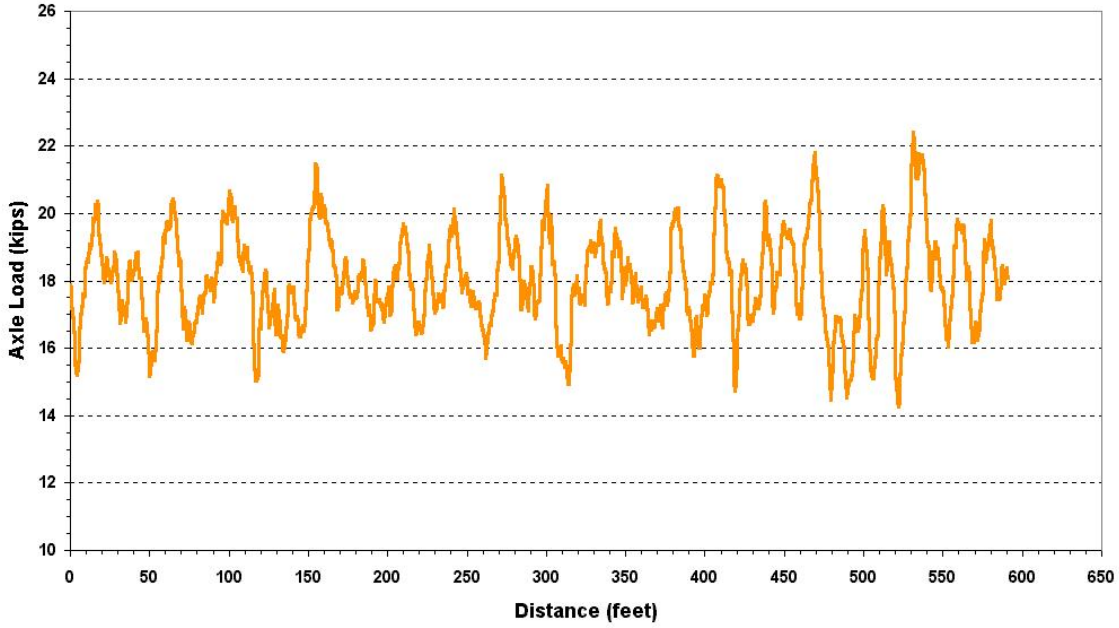

Figure A2. Predicted Dynamic Loads on a Medium-Smooth Pavement (SI = 3.4).

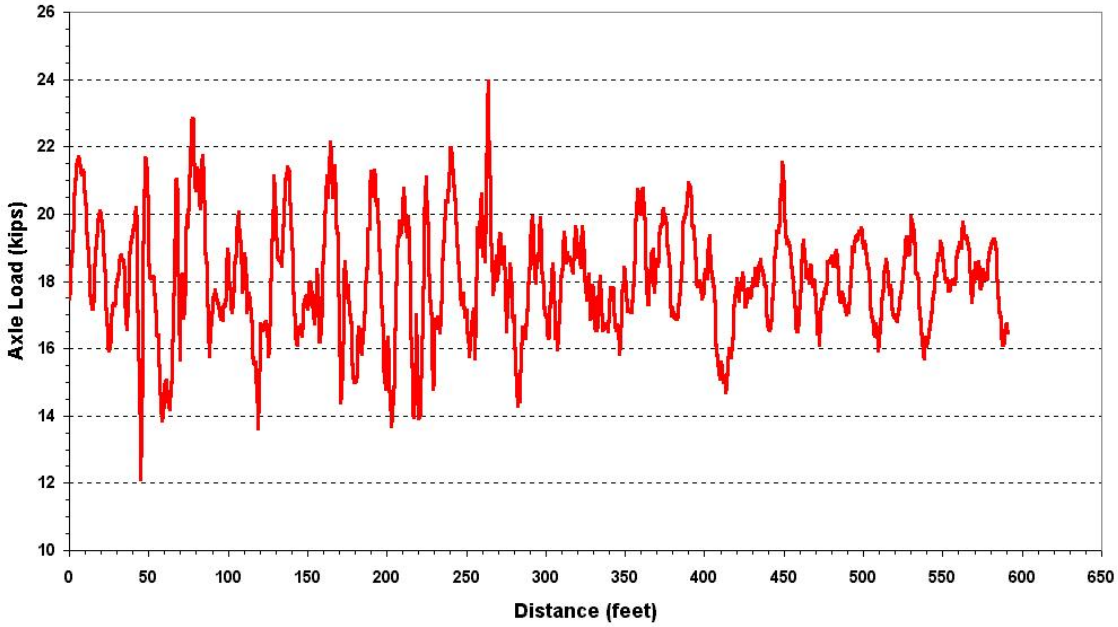

Figure A3. Predicted Dynamic Loads on a Rough Pavement (SI = 2.5).

The dynamic axle loads fluctuate about the static axle load, which corresponds to the mean of the predicted dynamic loadings. In the figures given, the static axle load is 18 kips corresponding to the standard single axle used in pavement designs currently implemented within state highway agencies. In the limit, if the surface profile is perfectly flat, the predicted dynamic loads would be a constant, equal to the static axle load, and the load profile would plot as a horizontal line. In this case, there will be no variability in the predicted axle loads. Because pavement response is directly tied to axle load magnitudes, it is logical to expect that dynamic axle load variations will lead to differences in predicted pavement performance.

Fernando (2002) proposed an index for evaluating the acceptability of overlay smoothness that is related to the predicted performance of the overlay based on reflection crack growth. To illustrate the concept underlying the development of this index, consider the two pavements shown in Figure A4. In the first case, a smooth overlay is built over the existing pavement, while in the second case, a rough overlay is constructed. Note that the underlying pavement is the same for both scenarios, as would be true for a given resurfacing project. Only the effect of differences in surface profile is considered. From theoretical considerations, Fernando (1998) developed an index for predicting the change in overlay life

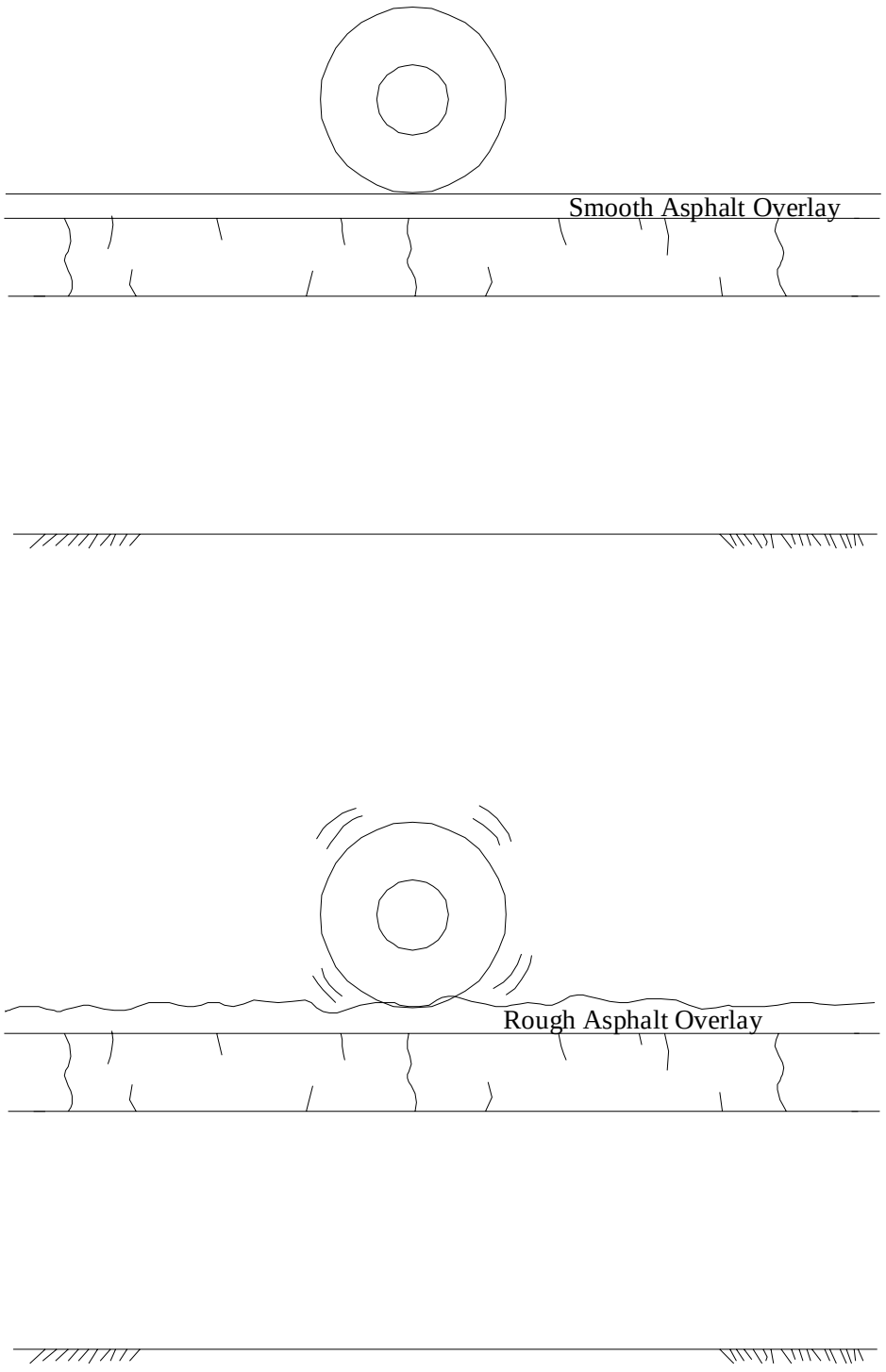

Figure A4. Illustration of Approach Used to Evaluate Initial Overlay Smoothness.

due to differences between the target and as-built surface profiles. It is given by the equation

$$\Delta = \left[\frac{1+z\,CV_0}{1+z\,CV_1}\right]^n - 1 \qquad \text{(A1)}$$

where

CV_0 = coefficient of variation of the applied dynamic wheel loads associated with the target profile from design,

CV_1 = coefficient of variation of the applied dynamic wheel loads associated with the as-built profile,

z = the number of standard deviations corresponding to a given percentile of the predicted dynamic load distribution, and

n = the exponent of the Paris-Erdogan crack growth law that affects the rate of crack propagation through the overlay.

The reader is referred to the report by Fernando (1998) for the derivation of Eq. A1. This equation provides a rational method for evaluating the quality of the finished surface on the basis of predicted performance. In practice, the coefficient of variation in Eq. A1 is determined by vehicle simulation using the measured profile. Note that Δ is related not only to the surface profile but to vehicle suspension and geometric characteristics, which all affect the variability in the applied dynamic wheel loads. The benefit of reducing this variability on predicted pavement life is readily apparent from Eq. A1. If $CV_1 < CV_0$, the predicted index is positive, indicating a predicted increase in pavement life with a smoother surface. Note that the reduction in wheel load variability is achieved not only by building smoother pavements but also by designing, manufacturing, and encouraging the use of trucks with improved dynamic performance. If the as-built and target profiles are the same, $CV_0 = CV_1$ and the predicted Δ is zero, indicating that the as-built surface meets the predicted service life associated with the target smoothness. Finally, if the as-built surface is rougher than the target, i.e., $CV_1 > CV_0$, Δ is negative, indicating a reduction in predicted pavement life because of the expected higher impact loading.

Huhtala et al. (1994) reported on the international roughness index developed by the World Bank in 1982 to classify road surface evenness. The IRI is determined from the longitudinal profile of the road, which is measured through a variety of methods. The IRI value of the measured profile is determined using the reference quarter car simulation model,

which has standard tire, suspension, and damper properties, and moves at a constant speed along the measured profile. The relative vertical displacement between the sprung and unsprung masses is calculated from the movements of the axle and body. The IRI statistic is then computed as the average of the computed relative displacements over a specified interval.

The road surface monitoring vehicle and Roadman were used to measure pavement profiles. The road surface monitoring vehicle was developed to meet the demand for fast and reliable measurement of road surface characteristics, permitting data collection at speeds of 40 to 90 kph (25 to 56 mph) with a daily measuring capacity of 100 to 400 km (62 to 249 miles). The test vehicle is fitted with beam-mounted ultrasonic distance sensors to measure the transverse profile at 2 m intervals. From the transverse profile, the depth of the rut, the height of the ridge between them, and the cross area of the rutting can be determined. A laser detector and accelerometer measure the longitudinal profile, which is then processed through the IRI quarter car simulator. Road geometry, which includes cross-fall, gradient, and curvature, is measured by gyroscopes and inclinometers. A visual inspection of surface distresses is conducted and entered manually in the computer.

The Roadman device measures the IRI values and also evaluates surface conditions. This device can be mounted in any passenger vehicle and consists of an accelerometer, pulse detector, and a central unit. The longitudinal profile is measured using an accelerometer, which is mounted on the axle beside the right wheel of the car.

A reported finding from this research is that the axle load of a heavy vehicle is not steady, but varies because the road is uneven. The dynamic axle load can be measured with an instrumented vehicle, simulated with computers, or measured locally by weigh-in-motion devices. The instrumented vehicle used for this study has three axles. The front axle has a leaf spring with dampers, and the tandem axle has a leaf suspension without dampers. The load is measured with strain gages at the ends of the axles, and the inertia effects are corrected with accelerometer measurements. With this configuration, the body pitch or bounce mode is much more important on the front axle, and axle hop mode is more important on the drive axle of the tandem axle.

Out of this research, it was determined that a new index was needed in addition to the IRI to describe how the dynamic axle loads due to unevenness of the road affect the life of a pavement. Therefore, the dynamic roughness index (DRI) was developed. For this purpose,

the quarter car model was used. Its parameters are the sprung mass, unsprung mass, suspension spring rate, tire spring rate, and the damping rate of the shock absorber. Four approaches were used to select a model to determine the DRI:

- spectral analysis of the road profile,
- maxima of dynamic axle loads,
- standard deviation of the axle loads, and
- application of the fourth power law.

Researchers found the fourth power law to be the most realistic and useful method for determining the DRI. Researchers computed the IRIs and DRIs from 140 profiles and found the correlation coefficient between these statistics to be 0.67. At an IRI value of 1.5 m/km, the DRI is between 100 and 140. At an IRI value of 3 m/km, the DRI is between 120 and 160. The researchers were of the opinion that useful information can be obtained from this index.

Chatti and Lee (2002) developed a new roughness index called the dynamic load index (DLI) in order to identify pavement profiles that were likely to generate high dynamic truck-axle loads. Previously, Chatti had developed relationships between dynamic axle loads and road roughness to confirm the existence of a critical roughness level that leads to the accelerated pavement damage. However, this development was based only on passenger car response to pavement roughness as measured by the ride quality index (RQI). Researchers realized that the majority of pavement damage is caused by heavy truck axle loads and that an accurate prediction of roughness level that would excite trucks required the evaluation of dynamic truck-axle loads likely to be generated by the profile characteristics of individual pavements. The new DLI negates the need for running a truck simulation program to determine whether a pavement profile is in need of smoothing based on truck dynamic loads.

Because a large portion of heavy vehicles have similar geometric and dynamic characteristics and tend to travel at similar highway speeds, spatial repeatability of dynamic loads is expected in normal traffic conditions. To investigate the spatial repeatability of the dynamic axle loads for all truck axles, the correlations between the different axles were studied. Because axle load variation is a function of the given pavement profile and truck characteristics, the coefficient of correlation between two axles for a given set of profiles is a good measure of spatial repeatability, which has been shown to be indicated by a correlation coefficient of 0.707.

The spatial repeatability of dynamic truck-axle load was analyzed using three different truck types – a two-axle single unit truck, a three-axle single unit truck, and a five-axle tractor semitrailer. Researchers used the TruckSim program to predict the dynamic axle loads generated by these trucks for 68 pavement profiles. All three truck types were equipped with standard flat lead suspensions, and default parameters in the TruckSim program were assumed. Researchers found that the best correlations between profiles for each axle load and those for the reference axle load were among the drive axles for all three trucks. The worst correlation was with the rear axle of the tractor semi-trailer, which indicates that the trailer was out of phase with the tractor. In these findings, it was determined that the second axle load in a five-axle semitrailer was representative of the three truck types. This reference axle was used to develop relationships between the RQI, DLI, and dynamic load.

The RQI was developed by the Michigan Department of Transportation in the early 1970s. Through a series of mathematical and statistical steps, the PSD was found to have a 90 percent correlation with subjective opinions of ride quality. From this finding, the method developed for computing RQI splits the profile into three wavelength bands. The index is then determined from these three wavelength bands using the equation

$$RQI = 3\ln(Var1) + 6\ln(Var\ 2) + 9\ln(Var3) \qquad (A2)$$

where

Var1 = the variance for 7.6 to 15.2 m wavelengths,

Var2 = the variance for 1.5 to 7.6 m wavelengths, and

Var3 = the variance for 0.6 to 1.5 m wavelengths.

An RQI value from 0 to 30 indicates excellent ride quality. RQI values from 31 to 54 indicate good ride quality. Values from 55 to 70 indicate fair ride quality, and values above 70 indicate poor ride quality.

However, researchers determined that a profile-based index focused on wavelengths in the 6.7 to 17.9 m range and the 1.8 to 3.3 m range would have a better correlation with truck dynamic axle loads than car response-based pavement roughness indices, such as the RQI and IRI. By examining the PSDs of dynamic axle loads on two rigid pavements with the same RQI but different dynamic loading coefficients, researchers confirmed that the dynamic truck axle load is related to profile elevations having wavelengths from 6.7 to 17.9

m, which excites the truck body bounce, and from 1.8 to 3.3 m, which excites the axle bounce.

The new profile index was found according to linear random vibration theory, in which the PSD of the truck response was obtained by multiplying the square of the truck response function by the PSD of the surface profile. The variance of the truck response was then found by considering only the frequency ranges of 1.5 to 4.0 and 8.0 to 15.0 Hz, which correspond to the truck and axle bounces, respectively. The variance V_y is determined from the following equation:

$$V_y = |G(w_1)|^2 V_1 + |G(w_2)|^2 V_2 \quad \text{(A3)}$$

where

$G(w_1)$ = peak value of truck response function in the frequency range of 1.5 to 4.0 Hz,

$G(w_2)$ = peak value of truck response function in the frequency range of 8.0 to 15.0 Hz,

V_1 = variance of the elevation in the frequency range of 1.5 to 4.0 Hz, and

V_2 = variance of the elevation in the frequency range of 8.0 to 15.0 Hz.

Based on the standard deviation of the truck response and Eq. A3, the new roughness index, DLI, is determined from the following equation:

$$DLI = \sqrt{a_1 V_1 + a_2 V_2} \quad \text{(A4)}$$

where

V_1 = variance of the profile elevation in the wavelength range of 6.7 to 17.9 m corresponding to a frequency range of 1.5 to 4.0 Hz for a truck traveling at 96 kph,

V_2 = variance of the profile in the wavelength range of 1.8 to 3.3 m corresponding to a frequency range of 8.0 to 15.0 Hz for a truck traveling at 96 kph, and

a_1, a_2= weighting factors.

For convenience, researchers set a_1 equal to one and a_2 equal to 14, the value that gave the highest correlation between DLI and dynamic loads. Therefore, the final equation for computing DLI is:

$$DLI = \sqrt{V_1 + 14 V_2} \quad \text{(A5)}$$

According to the researchers, the use of DLI is beneficial in the following ways:

- DLI can differentiate between profiles that generate high dynamic loads and those having the same RQI but generating low dynamic loads, and
- DLI can be used to decide the need for smoothing or correcting the profile of a given section without running a truck simulation program.

Papagiannakis and Raveendran (1998) developed the roughness index for driving expenditure (RIDE), which is compatible to the International Standards Organization (ISO) standard on "exposure to whole-body vibration." The two main requirements for the development of the index were that it be related to the riding comfort of passenger cars and heavy trucks and that it reflect the pavement roughness aspects that relate to the dynamic axle loads generated by heavy trucks. Papagiannakis demonstrated in previous research that the main contributor to the dynamic axle loads of heavy trucks is the vertical acceleration of the sprung mass with no dependence on suspension type. This work was done with instrumentation that measured both dynamic axle loads and sprung mass acceleration. Based on this research, it became evident that a pavement roughness index based on sprung mass acceleration would be preferable to one based on relative axle displacement, such as the IRI. It was also determined from previous research that the calculation of an index based on sprung mass acceleration is more efficient in the frequency domain than in the time domain, and that a frequency domain transfer function with a resonant frequency of about 3 Hz and corresponding amplitude of about 400 $m/sec^2/m$ is representative of the sprung mass response exhibited by both heavy trucks and passenger cars.

The transfer function that was selected to be used as a reference in calculating RIDE was determined from data obtained from an instrumented five-axle semitrailer truck on a pavement of medium roughness at 80 kph. This selection was made in order to provide a comparison to IRI, which is also calculated based on a speed of 80 kph. The power spectral density of the sprung mass acceleration response was found by multiplying the PSD of the pavement profile by the square of the reference frequency domain transfer function. The new index, RIDE, was then found by integrating the PSD of the pavement profile over the frequency range from 0 to 50 Hz. This gives the sum of the squares of the sprung mass acceleration response of the reference vehicle. The square root of this integral divided by the length of the pavement traveled results in a root-mean-square (RMS) of the acceleration response per unit length, which is compatible with ISO 2631.

Hassan and McManus (2003) developed a new pavement roughness index that represents the heavy-vehicle driver's perception of pavement rideability using existing profile data measured along the wheel paths of a passenger car. This was done by conducting an assessment survey to gather truck drivers' ratings of the ride quality of a number of road sections with various roughness levels along a highway in rural Victoria, Australia, on which there is a high percentage of heavy vehicle traffic. The data were then analyzed by correlating the mean panel rating (MPR) to roughness content in different wavebands of each road section. The roughness content that resulted in the highest correlation was then used in developing the new index referred to as the profile index for trucks (PI_t).

Researchers performed PSD analyses on the road surface profile data using the RoadRuf software developed by the University of Michigan Transportation Research Institute (1997). Profile data were converted into slope values by subtracting adjacent elevation readings and dividing by the sample interval. RMS values of profile slope in one-third octave bands were then determined. The MPR was correlated with roughness contents in different wavebands to identify wavelengths that influence ride perception. This analysis showed that the waveband between 4.88 and 19.51 m gave the highest correlation with the MPR. Thus, researchers used the roughness content in this band to establish the new index given below:

$$PI_t = \sqrt{\frac{(PI_{OWP})^2 + (PI_{IWP})^2}{2}} \qquad \text{(A6)}$$

where

PI_{OWP} = the average of the RMS values of the profile slope for the outer wheel path, and

PI_{IWP} = the average of the RMS values of the profile slope for the inner wheel path.

An exponential transform was also used to develop a truck ride number (TRN) to predict pavement ride quality, as perceived by heavy-vehicle occupants, from existing road surface profile data. This index is given by the following equation:

$$TRN = 5e^{-140(PI_t)^{0.84}} \qquad \text{(A7)}$$

Equation A7 gave the highest correlation coefficient between predicted TRN values and actual MPR values. Another TRN equation was developed using IRI as the predictor of

MPR. This alternative equation was also found to be a good predictor of MPR, but not as good as Eq. A7. The TRN equation based on IRI is given by:

$$TRN_{IRI} = 5e^{-118.70(IRI)^{0.9}} \quad \text{(A8)}$$

TRUCK TESTS ON INSTRUMENTED PAVEMENT SECTIONS

Steven and de Pont (1998) conducted research at the Canterbury Accelerated Pavement Testing Indoor Facility (CAPTIF) to investigate the relationship between the dynamic loadings produced by different suspensions and the resultant pavement performance. This research was done by comparing two different suspensions, whose performance characteristics were at opposite ends of the spectrum, with the simulated loading and vehicle emulator (SLAVE). The two SLAVE vehicles use standard heavy-vehicle suspension components, which are equipped with half-axle assemblies that can carry either single or dual tires. The SLAVE was fitted with suspensions similar to actual heavy-vehicle components, with one vehicle having an air spring suspension with hydraulic shock absorbers and the other having a multi-leaf steel spring.

After construction of a test pavement, 600 loading cycles of the SLAVE were applied to condition it before any testing was done. Transverse profiles were taken at each station, and longitudinal profiles were also measured with the Dipstick. The IRI values of the profiles were calculated from the longitudinal profiles and were found to be 4.8 m/km and 4.1 m/km for the inner and outer wheel paths, respectively. Tire deflections and imprints were measured at different applied load increments. Suspension stiffness was measured by recording displacements as load increments were applied to characterize the natural frequency and damping characteristics of the suspension.

The pavement started to show signs of deterioration at 60,000 loading cycles. The rate of deterioration slowed down after 105 loading cycles. After completion of 2.5×10^5 cycles, all of the H-bar gages in the asphalt pavement had failed because strains measured in the asphalt exceeded the capacity of the gages.

Researchers found that the pavement response was relatively constant during the experiment. The IRI values varied only slightly throughout the test, and the dynamic load coefficient (DLC) of the steel spring suspension is significantly higher than the air bag suspension. It was concluded that the effect of the steel spring suspension was an increase in the rate of pavement deterioration when compared to the air bag suspension.

Merrill, Blackman, and Ramdas (2002) conducted an international study to assess the significance of vehicle dynamic loading on the performance and maintenance costs of road pavements and bridges. This research arose from the results of a project, the Dynamic Interaction between Vehicle and Infrastructure Experiment (DIVINE), sponsored by the Organization for Economic Cooperation and Development, which was based on the limited testing of a few pavements and bridges. Also considered in this research were the results of the European Commission's Cooperation in Science and Technology (EC COST) Action 334, in which the effects of wide-single and dual tires on pavement wear were examined.

EC COST Action 334 considered the effects of wide-base single and dual tire assemblies on pavement damage, vehicle operating costs, vehicle safety and comfort, and the environment, especially noise. Particular attention was paid to the effects of single tires, wide-base single tires, and dual tires on pavement wear with respect to tire type and inflation pressure. The study conducted by Merrill et al. included the measurement of pavement response under dynamic loading, the measurement of contact stress distributions, and the assessment of pavement wear through trafficking. It was conducted at TRL's Pavement Test Facility (PTF). Equipment at this facility can traffic pavements with loads up to 100 kN (22.5 kip) at a maximum speed of 20 kph (12 mph) along a linear path.

Testing was conducted on a thin asphalt pavement, with a 100 mm layer of high density macadam (HDM) road base, and on a medium pavement, with 100 mm of HDM road base, 50 mm of dense bitumen macadam base course, and 50 mm of hot rolled asphalt surfacing. Both sections were constructed on 225 mm of unbound granular sub-base. Six tires were used in the study, which included four dual tires and two types of single tires. The tires used were:

- 495/45R22.5 Michelin Energy XDA wide-base single,
- 385/65R22.5 Michelin X XZA wide-base single,
- 295/60R22.5 Michelin X XDA dual pair,
- 295/80R22.5 Michelin X Pilote XDA dual pair,
- 315/70R22.5 Michelin X XDA dual pair, and
- 315/80R22.5 Michelin X Pilote XDA dual pair.

To measure the effects that different tire types, inflation pressures, and wheel loads have on the pavement structures, the subgrade was instrumented with soil strain gages placed

150 mm below the surface of the subgrade prior to laying the sub-base. These gages were oriented to measure the transient vertical compressive component of strain for all six tire types for a variety of loads and inflation pressures. The wheel of the heavy vehicle was also moved laterally to measure the strain in relation to the position of the load. Measurements were also taken at varying tire pressures, which ranged between 5 and 10 bars for each tire. The Tekscan Industrial Sensing (I-Scan) system was used to measure the load distribution for the different tire types at different loads and inflation pressures with a low resolution mat.

It was found that subgrade strains under the single tires diminish more rapidly as the tire moved away from the central position when compared to the dual tire assemblies. The difference was attributed to the differing contact areas in regard to the different tire types, but the difference diminished with an increase in pavement thickness. Inflation pressure had a negligible effect on subgrade strain, even with differentially inflated dual tires. Subgrade strain was measured with a change in load, and it varied linearly with both pavement thicknesses. However, the magnitude of the strain was higher for single tires than for dual tires. Also, the gradient of change was higher for the single tires than for the dual tires. In general, the pressure increased in the center of the contact areas for all tires with a negligible change at the edges of the tires. It was determined that the 385/65R22.5 Michelin X XZA wide-base single tire had a concentration of pressure in the center of the distribution, but the highest pressures are scattered. This difference was probably due to tread effects. The 495/45R22.5 Michelin Energy XDA wide-base single tire had three areas of high pressure, with a constant area of high pressure in the center and two areas closer to the edge of the tire. Also evaluated in this experiment was pavement wear under accelerated trafficking using the heavy-vehicle simulator at TRL and the two single tires. The following criteria were considered in this evaluation: rutting, deformation, subgrade stain, and cracking. The tires used for testing were loaded to 44 kN and to the manufacturers' recommended inflation pressures. Over 110,000 passes were applied to each pavement with the thinner pavement failing at 57,000 passes.

Deformation was measured at intervals during breaks in the trafficking using an optical level and measuring staff, which behaved as expected. Inferences were made from the deformation profiles in that there were fewer formations of small shoulders in the thin pavements on either side of the rut than for the thicker pavements. This observation indicated a punching action as opposed to a layer deformation. The ratio for the 385 to the

495 single tires on each pavement thickness showed that there was a much smaller difference between the two tire types on the thin pavement than on the thicker pavements. This was attributed to the failure of the thin pavement.

Rut depths were measured using straightedge and wedge, which differ from the optical levels because the reference point is not fixed and is a line that joins the two highest points over a 2-meter distance. Again, the rate of rutting was compared for the 385 and 495 single tires. The depth ratio reached 1.8 for the 100 mm pavement and reduced to 1.2 at the point of failure. The ratio for the 200 mm pavement reached 2.5 before reducing to 1.7 beyond 110,000 passes. The 200 mm pavement experienced about 40 percent less rutting with the 495 single tire than with the 385 single tire. Since no dual tires were tested in this part of the study, an attempt was made to estimate the likely outcomes for the accelerated testing with all tires.

Subgrade strain measurements were taken at the end of the trafficking and were compared to the measurements made at 2000 passes. The 100 mm pavement failed rapidly, and the strain increased by 5 times after 57,000 passes. The subgrade strain only doubled for the 200 mm pavement at 300,000 passes; however, there was significant difference between the two types of single tires.

Pavements were also monitored for signs of distress, such as cracking. The thin pavement for both tire types showed signs of distress after 15,000 passes, and the full length and width of the thin pavement were distressed after 30,000 passes. No visual signs of distress were observed for the 200 mm pavement.

Another part of this project accepted the detailed information available in regard to dynamic loading behavior with respect to the behavior of the vehicle. This study sought to link the contribution of dynamic loading by commercial vehicles to pavement wear in order to quantify the relationship between profile unevenness and the deterioration caused by dynamic loading effects, and in order to assess any significant repeat loadings on the development of localized deterioration. This objective was accomplished by examining the loading effects of actual commercial traffic on 10 in-service flexible and flexible composite pavements with a range of profile unevenness, commercial traffic, and structural strengths. Pavement deterioration was assessed from changes in longitudinal profile and rutting, and the dynamic loading was measured using an instrumented heavy goods vehicle.

The 10 sites were surveyed using a variety of equipment. These included an instrumented five-axle articulated lorry, TRL's high-speed survey vehicle (HSV), and the falling weight deflectometer (FWD). The instrumented lorry was used to measure the spatial repeatability and amplitudes of dynamic loading. The HSV uses laser sensors and a specially programmed computer to measure profile amplitude and wheel track rut depth, and the FWD was used to collect pavement deflection data. The results of this survey indicated a small but significant link between dynamic loading and change in road roughness.

The results of this research study show significant differences between tire types, but the thin pavements tested had some bearing on these results. The subgrade strain is significantly reduced with pavement thickness, so it was concluded that the effect of tire type on subgrade strain is negligible. The results of the accelerated trafficking tests showed that the 385/65R22.5 Michelin X XZA wide-base single tire consistently produced more wear than the 495/45R22.5 Michelin Energy XDA wide-base single tire under the same conditions. The rutting behavior was the most significantly affected by differences in tire types. Based on these results, it was determined that the single tires would have produced 1.5 to 2.5 times the deformation potential of the dual tires.

TRUCK SURVEYS

Wang and Machemehl (2003) conducted a survey to characterize in-service truck configurations on Texas highways. More specifically, they sought to characterize the in-service truck tire pressures on trucks and to identify factors that might be related to differences in tire pressure. To conduct this study, a three-factor factorial experiment was designed in which the state was broken up into six geographic regions. These regions were: Lubbock-Midland, Dallas, Houston, San Antonio-Austin, Corpus Christi, and the border areas. Also considered were two highway classes and two highway directions. A total of 623 trucks, classified according to the FHWA Truck Size and Weight Codes, were selected for the truck configuration survey and were tested for tire inflation pressure, tire temperature, tire size, and tire manufacturer.

Laboratory experiments and linear regressions were conducted on the data collected to establish the relationship between tire inflation pressure and tire temperature. The relationship determined by researchers is given by the following equation:

$$P_2 = P_1 + 0.22(T_2 - T_1) \quad \text{(A9)}$$

where P_1 and P_2 are tire inflation pressures in psi corresponding, respectively, to tire temperatures T_1 and T_2 in °F.

This study sought to characterize truck tire pressures across Texas and to verify if tire pressures were related to factors like geographic area, highway class, and highway direction. However, since tire temperature is directly affected by air and pavement temperatures, it was necessary to correct the tire pressure data to a standard temperature of 60 °C (140 °F) in order to characterize the relationship between tire pressure and tire temperature. In order to do this, researchers used the following equations:

$$P_2 = P_1 + \alpha \Delta T \quad \text{(A10)}$$

$$\alpha = \frac{P_1}{T_1} = \frac{nR}{V} \quad \text{(A11)}$$

where

R = ideal gas constant,
P_1 = gas pressure in atmospheres,
T_1 = absolute gas temperature in °K,
V = gas volume in liters,
N = number of gas molecules in moles, and
α = coefficient of the relationship between pressure and temperature.

To obtain values for α, inflated truck tires were tested at different temperatures in the laboratory, and a linear regression was run using the temperature and pressure data. The average α was found to be 2.73 kPa/°C.

A *t*-test was conducted to check whether there is a significant difference in tire inflation pressures between loaded and empty trucks. Table A1 shows the results of this test. The results indicate a significant difference in tire inflation pressures between loaded and empty trucks.

A *t*-test was also conducted on the effect of highway direction versus truck tire pressure. No significant differences were found. The effect of geographic region was found to match with the 1986 survey conducted by Roberts et al. Geographic regions were ranked in ascending order as follows: Border, San Antonio-Austin, Houston, Dallas, Corpus Christi, and Lubbock-Midland.

Table A1. Summary of *t*-test on Difference in Truck Tire Inflation Pressures between Loaded and Empty Trucks (Wang and Machemehl, 2000).

Test Group	Sample Size	Mean (kPa)	Standard Dev. (kPa)	Test Statistics	
435 loaded trucks	435 trucks	756.9	60.2	t=6.90	$Z_{95\%}$=1.96
169 empty trucks	169 trucks	718.2	69.1		

A one-way analysis of variance (ANOVA) was conducted for the comparison of border and non-border areas with respect to truck tire inflation pressure. The results of this test (Table A2) show a significant difference in tire inflation pressures between border and non-border areas, as indicated from the very small *p*-value given in the table. The low tire pressures in the border areas could be attributed to the North American Free Trade Agreement, which prohibits Mexican trucks from operating in the United States. More than 50 percent of the trucks selected in the border areas were empty.

A two-way ANOVA test was conducted to evaluate the effect of geographic area and highway class on truck tire inflation pressures. The results (Table A3) show the effects of geographic area and highway class to be significant, indicating that trucks in different geographical areas had different tire inflation pressures, and similarly for trucks in different highway classes.

A comparison was also made among the five axles of 500 3-S2 trucks selected using a one-way ANOVA. All tires of the same axle were pooled and averaged to represent the axle tire inflation pressure. The test results given in Table A4 show a significant difference among the five axles of the 3-S2s. The most significant of these results is that the first axle, which is the steering, possessed a much higher axle tire inflation pressure than the other four. Also, axles 2 and 3, which are the drive axles, possessed almost the same mean and variance values. Axles 4 and 5, which are the trailer axles, were different, but many of the trailers surveyed had a different license plate number than the tractor and were poorly maintained.

The study concluded that factors such as axle weight, tire temperature, geographic area, highway class, and axle type are related to tire inflation pressure. The results also suggest that trucks operating with high axle weights over long-haul distances traveling interstate highways with high operating temperatures will have higher tire inflation pressures in particular geographic areas. Lastly, it was determined that the steering axles have the highest tire inflation pressures of all the truck axles.

Table A2. One-Way ANOVA Results from Test of Difference in Tire Inflation Pressures between Border and Non-Border Areas (Wang and Machemehl, 2000).

Factor	Sample Size	Mean (kPa)	Standard Dev. (kPa)	Test Statistics	
Non-border areas	483 trucks	759.9	52.4	$F = 126.35$	$p = 0.000$
Border areas	140 trucks	695.9	78.7		

Table A3. Two-Way ANOVA Results for Geographic Area and Highway Class (Wang and Machemehl, 2000).

Factor	Test Statistics	
Geographic Area	$F = 11.58$	$p = 0.000$
Highway Class	$F = 14.74$	$p = 0.000$
Area × Highway Class	$F = 6.77$	$p = 0.000$

Table A4. One-Way ANOVA Results for Different Truck Axles (Wang and Machemehl, 2000).

Axle	Sample Size	Mean (kPa)	Standard Dev. (kPa)	Test Statistics	
1	499 axles	785.7	71.7	$F = 23.54$	$p = 0.000$
2	500 axles	751.3	73.5		
3	498 axles	750.4	72.4		
4	491 axles	752.9	78.9		
5	491 axles	743.6	83.4		